Design, Modelling, and Fabrication of a Hybrid Energy Harvester

by

Mohammed Ibrahim

A thesis

presented to the University of Waterloo

in fulfillment of the

thesis requirement for the degree of

Master of Applied Science

in

Mechanical Engineering

Waterloo, Ontario, Canada, 2014

Author's Declaration

I hereby declare that I am the sole author of this thesis. This is a true copy of the thesis, including any required final revisions, as accepted by my examiners.

I understand that my thesis may be made electronically available to the public.

Abstract

As sources of energy are becoming more scarce and expensive, energy harvesting is receiving more global interest and is currently a growing field. Energy harvesting is the process of converting ambient energy, such as vibration, to electrical energy that can power a multitude of applications. Vibration energy is the by-product of everyday life; it is generated from any perceivable activity. While typically viewed as noise, there is a strong potential for harvesting this energy and deploying it to useful applications. The focus of this thesis will be using vibration as the ambient source of energy.

Hybrid energy harvesters employ more than one of the harvesting technologies. In this thesis, two hybrid harvesters that utilize piezoelectric, magnetostrictive, and electromagnetic technologies are designed, modelled, and tested. Both of these harvesters have beams that are spiral in shape. The use of the spiral geometry allows the system to have a lower natural frequency as opposed to the traditional cantilever beam, while still maintaining a high volume of active material.

The first harvester that is discussed is the P-MSM harvester. It utilizes piezoelectric and magnetostrictive material. Both materials are configured in a spiral beam geometry and allowed to resonate independently. The resonance frequency of these two materials is designed to create wideband energy harvesting. This allows the harvester to be operating efficiently even if the ambient vibration shifts a small amount.

The second harvester that is discussed is the P-MAG harvester. It utilizes piezoelectric and electromagnetic technologies. It also incorporates a spiral geometry for the piezoelectric layers and includes a magnet attached at the centre. The magnet is placed in the centre of the spiral to reduce the natural frequency of the system and to also actively contribute to the harvesting. This harvester has two sources operating at the same resonant frequency, which allows it to have a larger power output than if the sources were separated.

Finally, finite element analysis was used to model both harvesters. ANSYS was used for the piezoelectric material and COMSOL was used for the electromagnetic material. The results are compared to the experimental and are in good agreement.

Acknowledgements

I would like to dedicate a special thanks to my supervisor Dr. Armaghan Salehian for her unyielding support and guidance during the program. I would like to thank and acknowledge Dr. Rafaat Mansour for generously providing access to the MEMS lab and FEA software.

Also I would like to thank members of my lab group, Tim Pollock, Blake Martin and Steven Lao for their continued assistance and support. In addition I would like to acknowledge the technical staff at the University of Waterloo specifically Andy Barber, Chris Mclean, and Richard Parker. I would like to thank Saman Nazari for assistance in the annealing process.

Last but not least, I would like to thank my family for their continued love, support, and encouragement during my graduate studies at the University of Waterloo.

Dedication

This thesis is dedicated to my mother and father whose sacrifice, love, and support have been the greatest inspiration in my journey.

Table of Contents

List of Figures

List of Tables

Nomenclature

A	cross-sectional area exposed to the magnetic flux
AWG	American wire gauge
B	magnetic flux density
c	damping coefficient
d_m	magnetostrictive strain coefficient
d_p	piezoelectric strain coefficient
D	electric charge displacement
E	electric field strength
EDM	electric discharge machining
EMF	electromotive Force
FEA	finite element analysis
FRF	frequency response functions
H	magnetic field intensity
k	spring stiffness
k_{ij}	piezoelectric coupling coefficient
m	mass
MEMS	micro-electro-mechanical system
MSM	magnetostrictive material
N	number of turns in a coil
NA	neutral axis
Nd:YAG	neodymium-doped yttrium aluminum garnet
NdFeB	neodymium
NPD	normalized power density
P	power output
PSD	power spectral density
PVDF	polyvinylideneflouride
PZT	lead zircronate titanate
s	mechanical compliance

S	strain
t	time
T	stress
V	volume
x	displacement of mass
$\dot{x}$	velocity of mass
$\ddot{x}$	acceleration of mass
y	displacement of base
$\dot{y}$	velocity of base
$\ddot{y}$	acceleration of base
β	damping coefficient
ε	dielectric permittivity
ε_o	dielectric permittivity in a vacuum
ε_r	relative dielectric permittivity
ζ	damping ratio
θ	angle between magnetic field and the area of interest
μ	magnetic permeability
ϕ	phase shift
Φ_B	magnetic flux
ω	frequency
ω_a	lower 3dB frequency
ω_b	upper 3dB frequency
ω_d	damped natural frequency
ω_n	natural frequency

Chapter 1: Introduction

1.1 Background and Motivation

Energy harvesting is the process by which energy is derived from ambient sources, captured, and stored for various applications such as small wireless autonomous devices (similar to those used in wireless sensor networks). As traditional energy sources continue to deplete the cost of their utilization continues to increase. This fact has generated a growing interest in energy harvesting on a global level. Figure 1 illustrates how a simple energy harvesting scheme is employed to convert and store ambient energy into electrical energy. The stored electrical energy can then be used by various sensor nodes for applications such as sensing, actuating, or sending wireless signals.

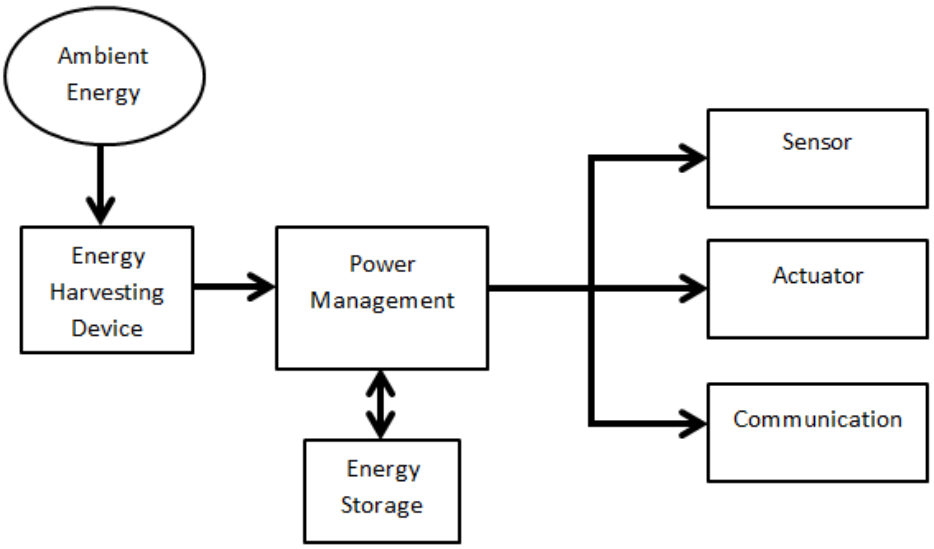

Figure 1: Generic sensor node architecture.

Solar, wind, and thermal energy are commonly used ambient energy sources for energy harvesting. Extensive research on both solar and wind energy sources has shown that they are capable of producing large power outputs, but suffer from a lack of scalability and indoor applications. Thermal energy harvesters derive energy from thermal gradients, such as a steam turbine, and are typically used alongside large scale technologies. Since the goal of this thesis is to design, model, and fabricate a small scale energy harvester, these previously mentioned energy sources are not applicable.

Kinetic energy is an example of another common ambient source of energy that is typically harvested using smaller-scale technologies. Although kinetic energy harvesters produce significantly less power

when compared to harvesters capturing other energy sources, recent advancements in electronics technology have allowed sensors to operate on far less power than in recent times. Some of today's low power electronics only require microwatts of power to be operational thus bridging the gap for ambient vibration energy conversion methods to become a viable power solution. Vibration energy is the by-product of everyday life; it is generated from any perceivable activity be it a motor rotation or human motion. While typically viewed as noise, there is the potential of harvesting this energy and deploying it to useful ends. The focus of this thesis will be using vibration as an ambient source of energy.

Some advantages of vibration energy harvesting include decreasing the cost of cabling and eliminating the need to constantly replace batteries. In addition, it allows the sensors to be embedded in locations that were previously restricted by these wiring limitations. It also allows the harvesters to be self-contained units with no required external power source, allowing for many more wireless solutions.

The foundation for vibration based energy harvesters can be modelled by a simple mass-spring-damper system as depicted in Figure 2. The basic equation of motion with base excitation is

$$m\ddot{x} + c\dot{x} + kx = -m\ddot{y} \tag{1}$$

where m is the mass, c is the damping coefficient, k is the spring stiffness, and x and y are the displacement of the mass and the base respectively. If the external excitation is sinusoidal, the steady state response will be

$$x = \frac{1}{\sqrt{\left(\frac{k}{m} - \omega^2\right)^2 + \left(\frac{c\omega}{m}\right)^2}} Ysin(\omega t + \phi). \tag{2}$$

where ϕ is the phase shift of the base input and Y is the amplitude. The fundamental natural frequency of the system is

$$\omega_n = \sqrt{\frac{k}{m}}. \tag{3}$$

A natural frequency of a system is the frequency at which the system will oscillate during free vibrations. If the system is subjected to a periodic input of similar frequency then the system will reach resonance. Most mechanical systems are designed to operate in a range as far from resonance as possible to avoid

destructive vibrations. Vibration based energy harvesters however are designed to operate as close to the resonant frequency of the ambient vibration source as possible to capture the large displacements that will be imposed on the system. Table 1 shows the values of some of the vibrations that are experienced on a daily basis.

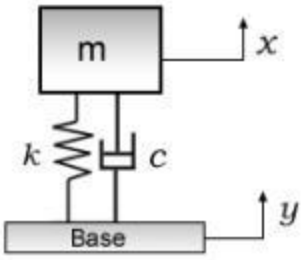

Figure 2: Mass-spring-damper system experiencing base excitation.

Table 1: Different sources of vibration and their respective frequency and acceleration.

Source	Acceleration $[m/s^2]$	Frequency $[Hz]$
Person tapping heel	3	1
Human walking	5-10	<20
Car instrument panel	3	13
HVAC vents in an office	0.2-1.5	60
Base of a 3-axis machine	10	70
Car engine compartment	12	200

This thesis will specifically focus on kinetic energy caused from unwanted ambient vibrations in structures and mechanisms. In recent years, substantial research has been conducted in this field; energy harvesting systems typically make use of electrostatic [1, 2, 3], electromagnetic [4, 5, 6, 7], piezoelectric [8, 9, 10, 11], and magnetostrictive [12, 13, 14, 15] transduction. These different technologies have been successfully tested and demonstrated in many institutions worldwide. In this thesis the electromagnetic, piezoelectric, and magnetostrictive technologies will be highlighted. The basic theory behind each of these technologies will be explained with the history of advancements made in the respective fields. Furthermore, a method for optimizing energy harvesting devices will be discussed by employing the use of multiple technologies together to create a hybrid system. This type of system has the potential to be more efficient and to cover a wider range of operating frequencies.

1.2 Thesis Organization

A basic overview of energy harvesting has been given thus far, along with an outline of different sources of ambient energy and different technologies that are used in vibration based harvesters. This section outlines the contents and scope of each chapter in this thesis.

Chapter 2 provides details on the field of energy harvesting from the literature. Previous works are explored to understand what has been performed and to assess their results. Hybrid harvesters are then explored to better understand which harvesting technologies have been coupled and analyze their effectiveness. From the information gathered, two hybrid devices are then suggested for modelling, fabrication, and testing.

Chapter 3 explains the basic physics principles of piezoelectric, magnetostrictive, and electromagnetic material along with their respective transduction mechanisms. The aim is to provide a better understanding of how these materials work in order to harvest energy and to lay the groundwork for the application of these principles throughout the rest of this thesis.

Chapter 4 explains the modelling of the two hybrid harvesters along with the procedure used to produce the simulation results. The configurations for both of the hybrid harvesters are modelled for stress, strain, and power output to provide a comparative base for experimental results.

Chapter 5 provides an explanation of the experimentation process. Details of the steps taken to design and fabricate the harvesters are discussed. The test setup and equipment used are highlighted. Lastly, the results of the output of both harvesters are displayed.

Chapter 6 brings together the simulation results from Chapter 4 and the experimental results from Chapter 5 to validate the theoretical model developed with the experimental results obtained. An explanation of any discrepancies is provided.

The thesis concludes with an overview of the results and performance of the harvesters. The benefits and drawbacks are highlighted and recommended improvements and future work is discussed.

Chapter 2: Literature Review

This thesis focuses on the electromagnetic, piezoelectric, and magnetostrictive energy harvesting technologies. Advancements in each of these areas will be discussed, as well as the use of more than one technology to create hybrid harvesters. Advantages of using hybrid harvesters with their respective pros and cons of each are discussed.

2.1 Electromagnetic

There has been substantial work done with electromagnetic energy harvesters that use Faraday's law of induction as the underlying principle of operation. Using the fundamental idea that a magnet moving inside a coil will induce a voltage, Saha et al. [16] developed an electromagnetic energy harvester. There are two fixed magnets at each end of the device, acting like springs, to produce a repulsive force on the moving magnet as it approaches either end. A similar design was used by Duffy et al. [17] where the electromagnetic energy harvester was incorporated in a shoe sole with the aim of gathering energy from human motion, which has frequencies of less than 30 Hz. An alternate design using repulsive forces was also considered by placing a coil in-between two magnets that were oriented such that they repelled one another. As the person would step down, the gap between the magnets decreased causing a change in the magnetic flux due to the increase in repulsive forces which induces a voltage in the coil. These devices are relatively large in size and interfere with the human motion and are therefore ineffective for the proposed application.

In the realm of wireless sensor application devices, a challenging task is to create energy harvesters that are substantially compact and produce appreciable power output. El-Hami [18] proposed a cantilever beam with two magnets attached to a c-shaped core. The purpose of such a core is to maximize the magnetic flux in the gap between the two magnets to induce the maximum amount of voltage in the coil. Although this configuration allows for a small (millimeter) footprint, it increases the natural frequency of the system to 322 Hz. This frequency is very high for the purposes of this thesis where the goal is to have a system with as low of a frequency as possible (less than 30 Hz) to capture vibrations from the ambient.

Different methods have been researched in an attempt to increase the power output of such devices. Beeby et al. [19,20] employed a similar cantilever beam system to that of El-Hami [18], but had four magnets arranged in such an orientation to maximize the magnetic flux gradient through the coil in the centre. The magnets were placed two on each side and were attached to a zinc coated mild steel keeper which couples the magnetic flux of the magnets. Although the size of this harvester was small, the added

weight of the magnets allowed it to resonate at a low frequency of 52 Hz. Even though this harvester exhibited a small size and low resonance, it was limited by the operating range and may only generate appreciable energy at its natural frequency.

Yang et al. [21] designed a harvester that operated at the first three resonant modes. It consisted of a pinned-pinned beam with three equally spaced magnets. Under each magnet was a planar coil that induced a voltage as the magnets vibrated. This device harvested energy from the first three modes located at 346 Hz, 958 Hz, and 1145 Hz respectively. Although having multiple harvesting frequencies was an improvement on previous devices, the high operating range is less than desirable in many applications.

To increase the range of operation, Soliman et al. [22] introduced a mechanical stopper that is in the range of motion of a cantilever beam. When the beam comes in contact with the stopper, the stiffness of the beam increases and will change the resonance frequency of the system. This harvester was able to harvest energy from 93 Hz to 102 Hz, making it a wide band energy harvester. Wide band energy harvesters maximize the system's ability to harvest energy from the environment.

Another method to increase the bandwidth was employed by Sari et al. [23]. The authors proposed a micro-electro-mechanical system (MEMS) device that consisted of numerous cantilever beams of varying lengths. This meant that each beam had a different natural frequency. On each beam was a copper wire coil which moves through the magnetic field of a fixed magnet a specific distance from the beam. The beams and the coils were connected serially. Essentially, this is similar to having multiple standalone energy harvesters working side by side to ensure a minimum of one subsystem being excited at any given time from the input vibration. This harvester also had a wide band harvesting range from 3400 Hz to 4400 Hz. This large operating range at such high frequencies was due to the size of the harvester but for applications sought by this thesis, it is not practical.

2.2 Piezoelectric

Piezoelectric energy harvesters have been gaining substantial interest due to their natural electro-mechanical coupling properties and the advancements that are being made in their design and fabrication. A basic configuration, widely-studied in the field of piezoelectric energy harvesters, consists of two piezoceramic layers bonded together and referred to a bimorph configuration in the literature. Roundy and Wright [24] proposed a cantilever beam made from a piezoelectric bimorph. The cantilever orientation allowed the material to be strained while the system underwent vibrations. Due to the piezoelectric properties, this strain produced an electric current which is harvested and used to power small devices.

The developed harvester is a basic cantilever beam with a tip mass. It is excited at 2.5 m/s^2 and has a natural frequency of 120 Hz. The piezoelectric cantilever beam has been modelled in various works, see [25, 26].

The standard rectangular cantilever beam has an uneven strain distribution with the maximum strain occurring near the clamped end. White et al. [27] proposed a stainless steel tapered base with two layers of piezoelectric film printed on both sides. The tapered shape was used to allow for even strain distribution throughout the entire beam. This maximized the deflection of the piezoelectric layers which in turn maximized power output.

Similar to the harvesters discussed in the previous section, the cantilever beam configuration only works at a specific frequency. In order for these harvesters to be used in real application they must possess a wider operating range. Challa et al. [28] proposed a system in which the natural frequency could be passively tuned to match the source frequency. The configuration consisted of a piezoelectric cantilever beam with a tip mass and magnets on both sides of the free end. There was also a set of fixed magnets that surrounded the beam. The distance of these magnets was altered which resulted in a perpendicular magnetic force on the beam, altering the beam's stiffness and changing the natural frequency. By varying the distance of the fixed magnets, this device could be tuned in the frequency range of 22 Hz to 32 Hz.

Another work by Mansoura et al. [9] used magnets to apply a tensile stress on a beam, altering the stiffness and thus changing the natural frequency of the harvester. It was observed that the tuning range of this harvester was from 3.19 Hz to 12 Hz. However this tuning range came at the expense of reduced power output due to the stiffening of the beam. Leland and Wright [29] had similar results while applying a mechanical axial load to a pinned-pinned piezoelectric bimorph. These three designs [9, 28, 29] were all tuneable before operation however, as with non-wide band harvesters, their main drawback is that once the frequency is set it cannot be changed.

With the knowledge that energy harvesters are most efficient under resonance, one must design the beam to have the natural frequency near the ambient frequency. Studies have been performed that show the typical vibrations that occur in locations where wireless sensors would typically be located. Examples are an engine compartment and an HVAC vent in an office building which ranged from 0.2 to 10 m/s^2 at frequencies below 60 Hz [8]. This means the natural frequency of the harvester should be low enough to match these values. In cantilever beam configurations, either the length or the tip mass is increased to lower the natural frequency. This poses a physical limit in the configuration process due to the need of decreased size for the harvesters. Hu et al. [30, 31] proposed a novel configuration of a piezoelectric beam with the shape having less stiffness than the cantilever beam. The authors developed a spiral piezoceramic

beam, which was fixed in the center and was subjected to a one newton force excitation. After testing it was observed that the beam had a natural frequency of 50 Hz. Paprotny et al. [32] continued with this idea and proposed a quad folded cantilever design that harvested energy from the magnetic field emanating from a current carrying wire. This harvester's unique design allowed for a natural frequency of 60 Hz.

2.3 Magnetostrictive

A growing interest is starting to form around materials that exhibit the Villari effect, known as magnetostrictive materials. This type of material has a coupling between the mechanical and the magnetic domains. As the material is deformed the magnetic polarization changes and conversely the material is deformed when a changing magnetic field is applied. A common magnetostrictive material is Terfenol-D. It has an ultra-high coupling coefficient and is generally used as an actuator to strain piezoelectric material which then produces a voltage. The most common application uses 2 layers of Terfenol-D to sandwich a piezoelectric layer. A changing magnetic field is then applied to this configuration causing the Terfenol-D to strain, which causes the piezoelectric layer to strain [33, 34, 35].

Minimal research has been performed using this material to harvest energy. Terfenol-D is extremely stiff and brittle and cannot be used in vibration based harvesting. Metglas is a thin film magnetostrictive laminate that is extremely flexible compared to Terfenol-D, due to its construction. Wang and Yuan [36] were the first to use Metglas for energy harvesting and used 8 magnetostrictive laminates on a bronze cantilever beam. This setup had a copper coil wrapped around it and through Faraday's law of induction, voltage was induced from the deformation of the Metglas layers. The fundamental resonance of this system was at 58 Hz, confirming the flexibility of this material.

2.4 Hybrid

All the works that have been cited in the previous sections present different methodologies to tune and improve different energy harvesting devices. The main objective in this field of research is to harvest as much energy as possible while maintaining a relatively small footprint. Traditionally, energy harvesting devices use only one of the above mentioned technologies. A method that is gaining more popularity recently is the creation of hybrid energy harvesting devices. Hybrid energy harvesting devices combine more than one of these technologies together to create a more efficient unit. The focus of this thesis will be in hybrid technologies from piezoelectric and electromagnetic technologies.

The simplest integration of these technologies was seen in the work of Wischke et al. [37]. They proposed a piezoceramic bimorph cantilever beam configuration with magnets acting as the tip mass. As the beam

vibrated the magnets passed through a coil. This is unique because not only are two different technologies being used but each has its own resonance. If tuned appropriately, this type of hybrid technology can be very effective in harvesting energy over a wider band. An effort was also made to use the energy harvested by the magnet to tune the piezoelectric stiffness.

Karami [38] developed a similar cantilever beam with piezoelectric patches near the base. The tip mass was also a magnet but had a unique configuration that interacted with a fixed magnet to induce voltage in a coil between them. The piezoelectric patches and the magnets attached at the tip both harvested energy separately. This harvester had a natural frequency of roughly 10 Hz and was capable of such a small resonance due the large size of the beam (152 mm in length).

Similar concerns regarding the size arise due to the required dimensions of the cantilever beam configuration in an attempt to lower the natural frequency of the device. Wu et al. [39] proposed a MEMS sized device with a unique shape for the piezoelectric beam to lower the natural frequency. The authors used four uniquely shaped piezoelectric springs and suspended a magnet from four sides. A fixed coil was located in the centre of the suspended magnet and as the system vibrated a voltage was induced. The piezoelectric springs were designed to reduce the natural frequency of the structure and contribute to the energy harvesting process.

2.5 Proposed Designs

The goal of this thesis is to design hybrid harvesters that operate at low frequencies in an attempt to capture ambient energy that typically has frequencies smaller than 30 Hz (such as human motion). In an attempt to combine materials that would improve the overall efficiency of the hybrid harvester, Table 2 highlights the major advantages and disadvantages of the technologies that were previously discussed. There are three possible combinations, piezoelectric-magnetostrictive, electromagnetic-magnetostrictive, and piezoelectric-electromagnetic.

Table 2: Advantages and disadvantages of different energy harvesting technologies.

Material	Advantage	Disadvantage
Piezoelectric	- high coupling - scalable (MEMS) - large output voltage	- chance of depolarization - brittle - high output impedance
Electromagnetic	- simple modeling - affordable material	- not very scalable - small output voltage - larger mass
Magnetostrictive	- highly flexible - high or low frequency vibration - ultra-high coupling	- requires bias magnets - nonlinear behavior - harder to model

Analyzing these three combinations with the data presented in Table 2, it is observed that the first combination (piezoelectric-magnetostrictive) has good potential due to the fact that these two materials complement each other's weaknesses. The piezoelectric material is brittle but produces high voltages and has high input impedance. On the other hand, the magnetostrictive material is very flexible and can withstand harsh environments while still maintaining ultra-high coupling.

The second combination (electromagnetic-magnetostrictive) will not match effectively because both of these technologies require a pick-up coil and rely on Faraday's law of induction. This means that the magnetic fields would interfere with each other potentially causing destructive interference, impacting the effectiveness of the pick-up coil. Consequently, this combination of technologies would negatively impact the quality of the voltage induced in the coil.

The third combination (piezoelectric-electromagnetic) also has good potential since the technologies harvest energy in different domains and will not interfere with each other. The output of each harvester could be added separately after the conversion to increase the output of the overall harvester since they can each operate in separate domains. Electromagnetic technologies are relatively simple to apply and model; combined with piezoelectricity it can be very effective.

Proposed in this thesis are two hybrid energy harvesting units that employ two different technologies. The first design (P-MSM) includes piezoelectric and magnetostrictive technologies, and the second design (P-MAG) employs piezoelectric and electromagnetic technologies.

The piezoelectric component in both designs will be a spiral shaped piezoelectric bimorph (shown in Figure 3 below). The spiral shape will produce a unit with smaller stiffness and therefore will have more deflection as opposed to the traditional cantilever beam or circular disk configurations. Also, the spiral shape has the potential of being incorporated into MEMS scale applications due to the fact that it can have a low natural frequency even at small sizes [40].

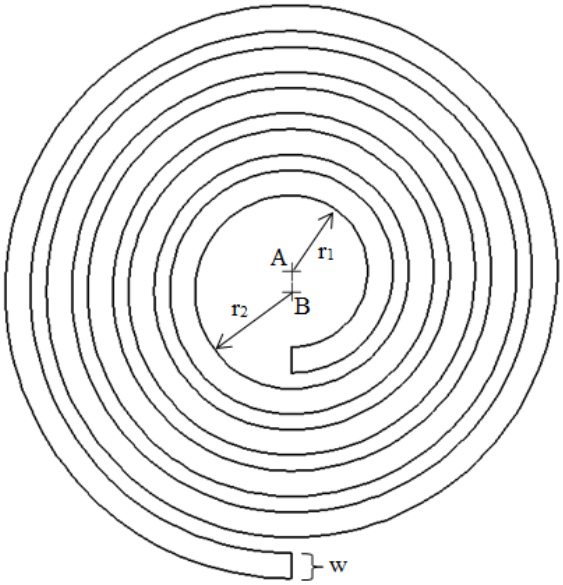

Figure 3: Spiral shaped beam.

The first design, the P-MSM harvester, incorporates the piezoelectric spiral bimorph and a magnetostrictive layer also in a spiral geometry as shown in Figure 4. Each of the layers is fixed at the point of contact with the mount and the center is allowed to move independently of each other. When the magnetostrictive material is strained, it introduces a change in the magnetization of the material. When a copper wire coil experiences this change in magnetic field caused by the strain of the magnetostrictive layer, then through Faraday's law of induction a voltage will be induced in the coil which can be harvested. This concept can be seen in Wang and Yuan's [36] work. The advantage of this design is the potential to be very compact and be incorporated in many applications.

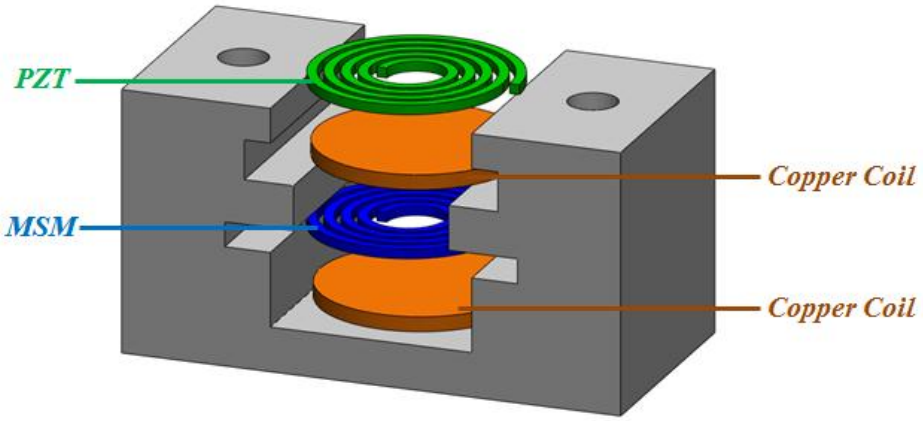

Figure 4: P-MSM design concept.

The second proposed design, the P-MAG harvester, incorporates a piezoelectric spiral beam with a magnet attached at the centre (refer to Figure 5). Note that the dimensions of the piezoelectric spiral beam in both the P-MSM and P-MAG harvesters are the same. The piezoelectric layer is fixed at the points of contact with the mount and as the system vibrates, due to the spiral shape, it will experience deflection in the centre. Therefore, the magnet that is attached to center of the piezoelectric spiral will also move inducing a voltage in the copper coil through Faraday's law of induction. Both the spiral beam and the copper wire will actively contribute to the energy harvesting process.

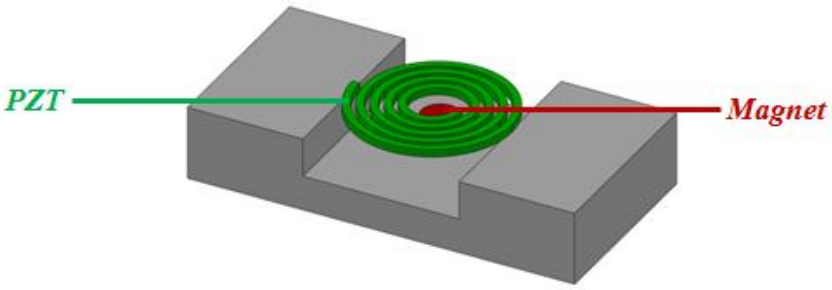

Figure 5: P-MAG harvester concept.

The P-MSM and the P-MAG harvester will be designed, constructed, and tested in this thesis. The results of each harvester will be highlighted and analyzed to determine the effectiveness of this hybrid strategy.

Chapter 3: Basic Theory

This chapter introduces the basic constitutive equations for the materials that are used in the proposed energy harvesters. The goal is to provide a better understanding of the properties of these materials and the potential they have to offer. Furthermore, different configurations and material types will be discussed.

3.1 Piezoelectric

Piezoelectric material is a type of smart or active material that exhibits a coupling between the mechanical and electrical domains called electromechanical coupling. Applying a force on the material generates a stress, which in turn results in deformation of the material. The deformed form will produce charge flow across the material, resulting in a voltage. The reverse effect also holds. For this reason it can be used for both sensing and actuation applications. Lead zircronate titanate (PZT) is a common piezoelectric material used today.

The mechanical behavior of piezoelectric materials is described by Hooke's law,

$$S = sT \tag{4}$$

where T is the external stress applied to the material. Due to this stress the material will elongate. The total elongation divided by the original length is defined as the strain, S. Stress and strain are related by the compliance of the material, s, which is the inverse of the Young's modulus of elasticity.

The electrical behavior of linear dielectric material is described by

$$D = \varepsilon E \tag{5}$$

where E is the electric field strength and D is the electric charge displacement. They are linearly related through the dielectric permittivity, ε. Materials are often expressed in terms of the relative permittivity, ε_r. The relationship with the dielectric permittivity is

$$\varepsilon = \varepsilon_r \varepsilon_o \tag{6}$$

where ε_o is the permittivity in a vacuum which is the minimum value of permittivity that can exist.

$$\varepsilon_o = 8.85 \times 10^{-12} \frac{F}{m}. \tag{7}$$

Combining Eq. (4) and Eq. (5) and expressing them in matrix form will yield

$$\begin{Bmatrix} S \\ D \end{Bmatrix} = \begin{bmatrix} s & d_p \\ d_p & \varepsilon \end{bmatrix} \cdot \begin{Bmatrix} T \\ E \end{Bmatrix} \tag{8}$$

where d_p is the piezoelectric strain coefficient. This is the coefficient that creates the electromechanical coupling. If d_p is equal to zero, then Eq. (8) will result in two decoupled equations each representing its own domain. The larger this value, the larger the effect of the electromagnetic coupling.

3.1.1 Material Types

There are several different types of piezoelectric material. In order to compare their respective energy harvesting capabilities the piezoelectric coupling coefficient, k, is commonly used. This coefficient describes the coupling between the two domains as shown in Eq. (9).

$$k_{ij} = \frac{d_p}{\sqrt{s\varepsilon}} \tag{9}$$

The subscripts denote the directions that are being considered. The first number represents the face of the element and second number represents the axis on that specific face. The number "3" indicates the poling direction of the material as displayed in Figure 6.

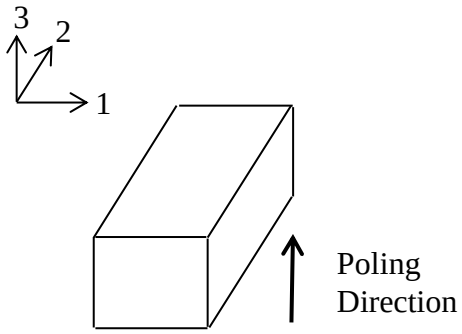

Figure 6: Poling of piezoelectric material.

These coupling coefficients measure the efficiency of each specific material in transferring energy between the mechanical and the electrical domain in each of the specified directions. While the

coefficients do not specify the actual efficiency of the materials, they provide an indicator through which materials can be compared. The subscript "33" is out-of-plane, and the subscript "31" is in-plane. Some of the common piezoelectric materials are shown in Table 3 [41].

Table 3: Comparison of different types of piezoelectric material [41].

Material	k_{33}	k_{31}
PZT-5A	0.72	0.35
PZT-5H	0.75	0.44
PVDF	0.16	0.11
MFC	0.69	N/A

Polyvinylideneflouride (PVDF) is the most flexible but has a very low coupling. PZT on the other hand is brittle but is generally the preferred material for vibration based harvesters due to its high coupling coefficient [42].

3.1.2 Configuration

There are two possible configurations for PZT material. One is simply using a single layer of PZT material, while the other is called a bimorph, which consists of two layers of PZT.

Figure 7 illustrates a cantilever beam with the neutral axis (NA) highlighted. At the NA, the beam experiences zero stress and strain. If the beam is bending upwards, then above the NA the beam will be in compression, and below the NA the beam will be in tension.

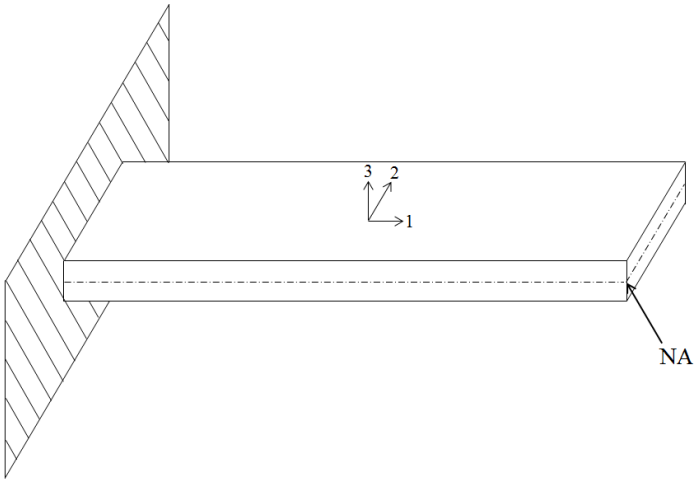

Figure 7: Cantilever beam with the neutral axis (NA) highlighted.

If the beam consisted of a single layer of piezoelectric material, the top half of the beam would produce a voltage and the bottom half would produce the same voltage but with an opposite sign. As expected, they will cancel each other out and will result in zero net output voltage from the overall beam.

On the other hand, if the cantilever beam consisted of two piezoelectric layers, referred to as a bimorph beam, the layers would have the exact same properties and geometry and will result in the NA being exactly in between them. In this case, if the beam is bending upwards then the top layer would be fully in compression and the bottom layer would be fully in tension. This results in two layers that produce opposite voltages, similar to having two different voltage sources.

It is clear that a bimorph configuration is advantageous for harvesting energy due to the fact that if a single layer is employed the voltage output will be zero. The bimorph configuration is generally used with vibration based harvesters [43, 44].

3.1.3 Poling Direction

Referring back to the analogy that was made earlier about the bimorph beam acting as two separate voltage sources, the sign of each source is determined by the poling direction of the layers. Figure 8 depicts a parallel connection in which both layers are poled in the same direction and the poling direction indicated by the arrows. One layer will be in compression and another layer will be in tension during vibrations causing the voltage output from each layer to have opposite signs. Figure 9 shows the equivalent circuit if the layers were modelled as a voltage source. In this configuration both sources always have opposite voltage output, which will result in flow shown Figure 9.

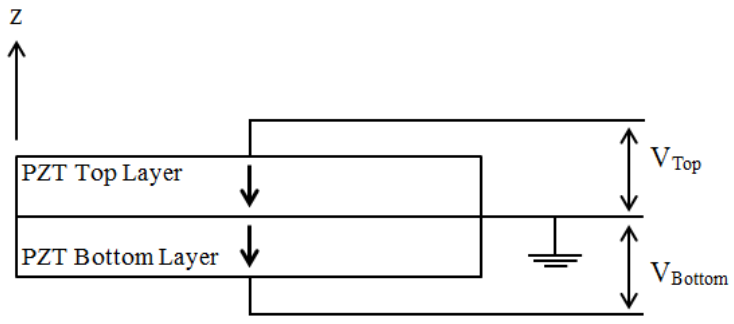

Figure 8: Parallel connection.

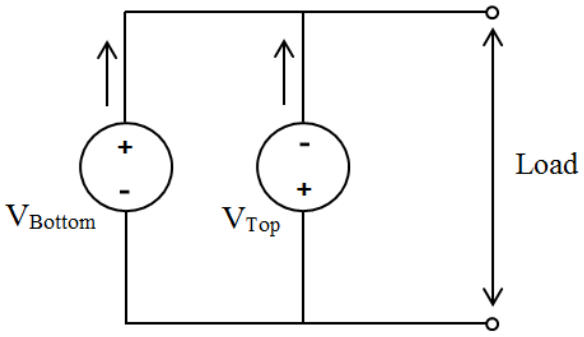

Figure 9: An analogy for the piezoelectric parallel circuit.

On the other hand, when the piezoelectric layers are poled in the opposite direction as depicted by the arrows in Figure 10, one layer will be in compression and the other layer will be in tension thus producing same-sign voltage outputs from each layer. This will act simply as two voltages sources in series, as shown in Figure 11.

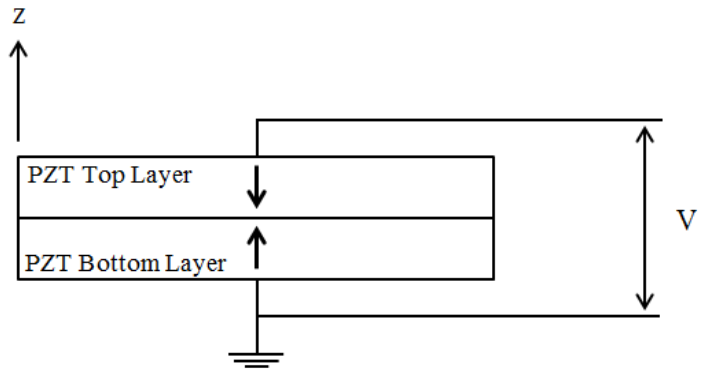

Figure 10: Series connection.

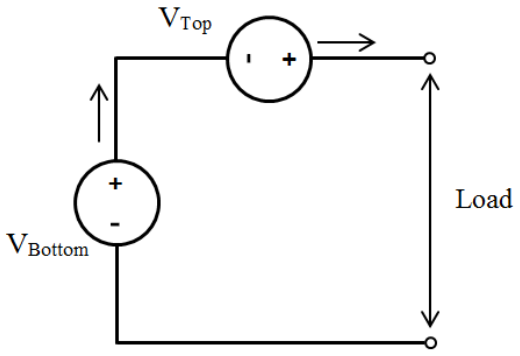

Figure 11: An analogy for the piezoelectric series circuit.

Rectifying circuits used to smooth the signal coming out of the harvester typically have a voltage drop across them due to some of the components used (such as diodes). It is thus favorable to have a higher voltage output for energy harvesting application in order to allow for some potential losses. The series configuration will output twice as much voltage as the parallel configuration. Based on this, the harvesters proposed in this thesis will be prototyped in a series configuration.

3.2 Magnetostrictive

Magnetostrictive material is a type of smart or active material that exhibits a coupling between the mechanical and the magnetic domains. When the material is subjected to mechanical stress it changes its magnetic polarization, which is known as the Villari effect. The reverse effect also holds.

Similar to piezoelectric material, the mechanical properties are described by Hooke's law (recall Eq. (4))

$$S = sT \tag{4}$$

where T is the external stress and S is the strain. They are both related by the compliance of the material, s.

The magnetic properties are related by

$$B = \mu H \tag{10}$$

where H is the magnetic field intensity and B is the magnetic flux density. These are related by μ, the magnetic permeability of the material.

Combining Eq. (4) and Eq. (10) in matrix form will yield

$$\begin{Bmatrix} S \\ B \end{Bmatrix} = \begin{bmatrix} s & d_m \\ d_m & \varepsilon \end{bmatrix} \begin{Bmatrix} T \\ H \end{Bmatrix} \tag{11}$$

where d_m is the magnetostrictive strain coefficient. Eq. (11) is the constitutive equation for magnetostrictive materials. It is very similar to the piezoelectric constitutive properties; the difference being that it utilizes the magnetic domain equation rather than the electric domain equation.

3.3 Electromagnetic

The final component of the proposed harvesters is the electromagnetic component. This will entail a moving magnet with a nearby pick-up coil. The basic principle of this operation is explained by Faraday's law of induction.

Faraday's law states that if a current carrying conductor experiences a changing magnetic field then a voltage (electromotive force) will be induced in this conductor. A wound up copper coil is an example of a conductor. The change could be produced by changing the magnetic field strength, moving a magnet toward or away from the coil, moving the coil into or out of the magnetic field, or rotating the coil relative to the magnet.

An experiment commonly used to illustrate the concept of Faraday's law of induction consists of a coil attached to a galvanometer and a moving magnet. When the magnet is moving the galvanometer deflects depending on the motion, and when the magnet is stationary no voltage is induced in the coil.

The equation for the induced electromotive force (EMF) is given by Eq. (12).

$$EMF = -N\frac{d\phi_B}{dt} \tag{12}$$

EMF is the induced voltage in the coil, and it is proportional to the negative rate of change of the magnetic flux ϕ_B. N is the number of turns in the coil.

The magnetic flux is defined as

$$\phi_B = B \cdot A = BAcos\theta \tag{13}$$

where B is the magnetic field and A is the area through which it passes. The angle between the magnetic field and the normal of the area is defined as θ.

Chapter 4: Modelling

This chapter outlines the design and configuration of the spiral beam geometry that is used throughout this thesis. A finite element analysis (FEA) is used for modelling the P-MSM and P-MAG harvesters. The results of these simulations are extracted for analysis and comparison with experimental results in Chapter 6.

4.1 Spiral Beam

Both of the proposed harvesters use a spiral beam configuration for the piezoelectric and magnetostrictive material components. The dimensions of the spiral are shown in Figure 12 below. As depicted in the figure, the largest dimension of the beam is less than 45 mm which makes this beam compact in size and will have low natural frequencies as proven by Hu et al. [30, 31].

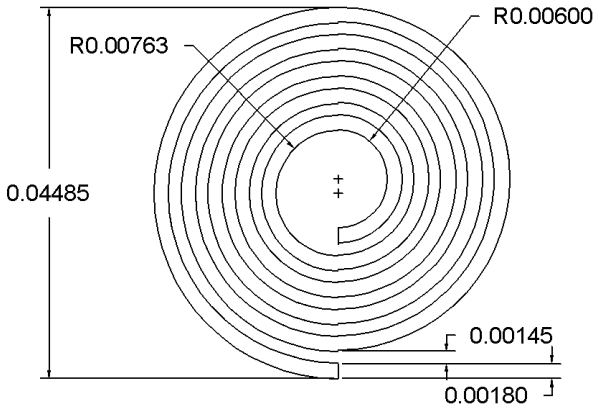

Figure 12: Dimensions of spiral beam. All dimensions are in mm.

The piezoelectric bimorph that forms the spiral is made up of two layers in a series connection as depicted in Figure 10 in the previous section. The direction of the arrows indicates the direction of polarization of the material. In a series connection, when one layer is in bending the other would be in compression so that when they both have opposite poling they will output a voltage with the same phase. This connection allows for the highest output voltage.

4.2 P-MSM

The P-MSM harvester is constructed with both piezoelectric and magnetostrictive materials. Only the piezoelectric spiral was modelled on ANSYS.

4.2.1 Piezoelectric Model

A finite element model of a spiral piezoelectric bimorph is made in order to analyse the structure and to validate the experimental results. ANSYS Mechanical APDL 14.0 was used for the piezoelectric spiral analysis. A 3-dimensional harmonic analysis was run to determine both the deflection and the voltage output of the piezoelectric spiral bimorph.

The full harmonic solver was used with element type Solid 266 with KEYOPT(1) = 1001 to activate the electromechanical coupling. It is a coupled field 20 nodes brick element. The top and bottom layer are made to be electrode layers where the measuring will take place. The two middle layers are electrically connected. The mesh was made up of 12,320 elements (refer to Figure 13 below). The frequency sweep went from 10 to 100 Hz with a constant out of plane acceleration of 0.3g. Figure 13 shows the boundary conditions where the nodes in the areas covered by the yellow boxes are fixed in the x, y, and z axes and the centre of the spiral is free to deflect. This is similar to a pinned-pinned beam condition.

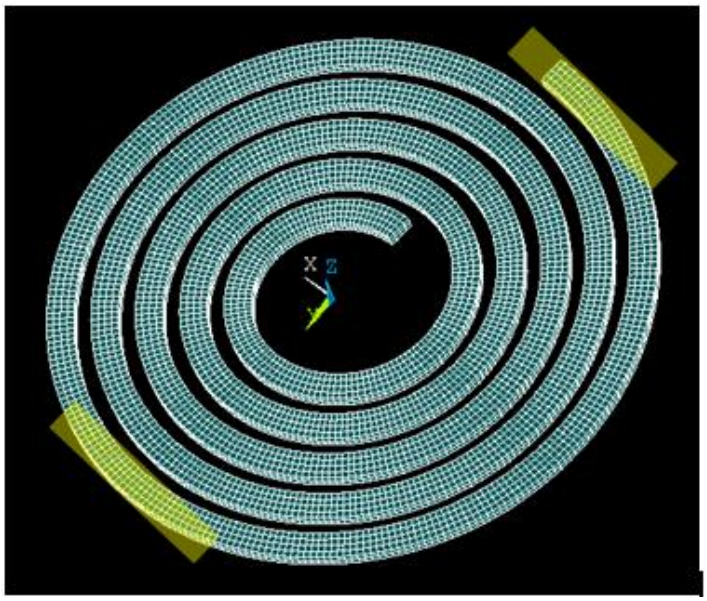

Figure 13: The elements of the mesh of the ANSYS simulation and highlighted in yellow are the fixed boundary conditions.

The displacement sensing location is chosen to be the centre of the spiral. Running this simulation produces the results shown in Figure 14. The first resonance of this beam is at 25 Hz, which is significantly less than the cantilever beam harvesters discussed in previous sections. The proposed method of reducing the natural frequency of the system by using a spiral beam geometry is therefore validated.

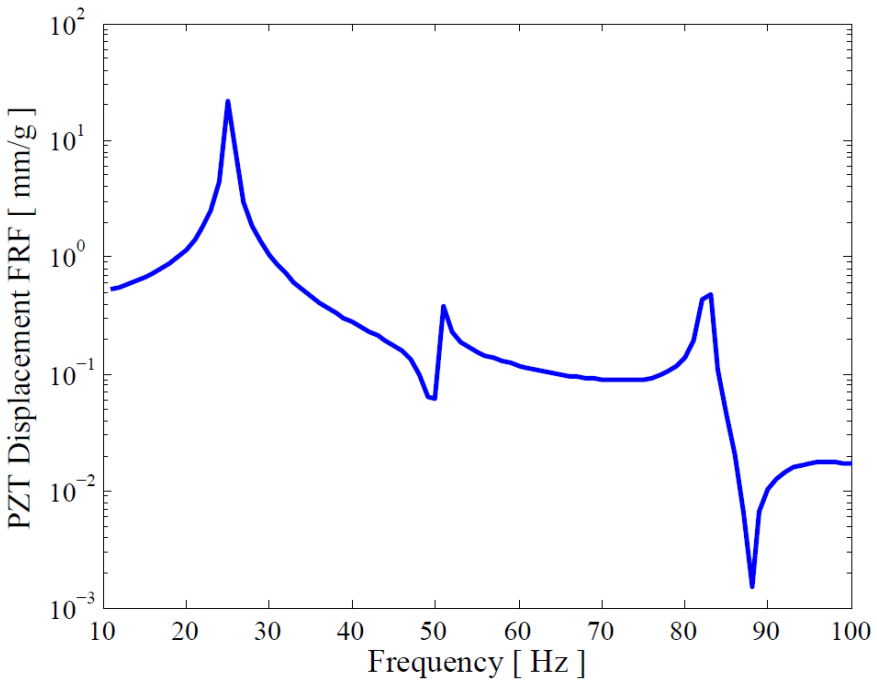

Figure 14: Displacement of the tip of the piezoelectric bimorph.

The simulated spiral beam in ANSYS can also be used to better understand the mechanics in order to fabricate and test a real setup. Most importantly, the stresses in the beam should be low enough so that it will not break or crack from the forcing function (input acceleration). Figure 15 shows a contour plot of the von Mises stress on the spiral piezoelectric beam, which is used to predict yielding of the material. As expected, the maximum stress occurs right after the boundary condition. From the results of this simulation, it is observed from the results of the ANSYS simulation that the beam will not break under this forcing function.

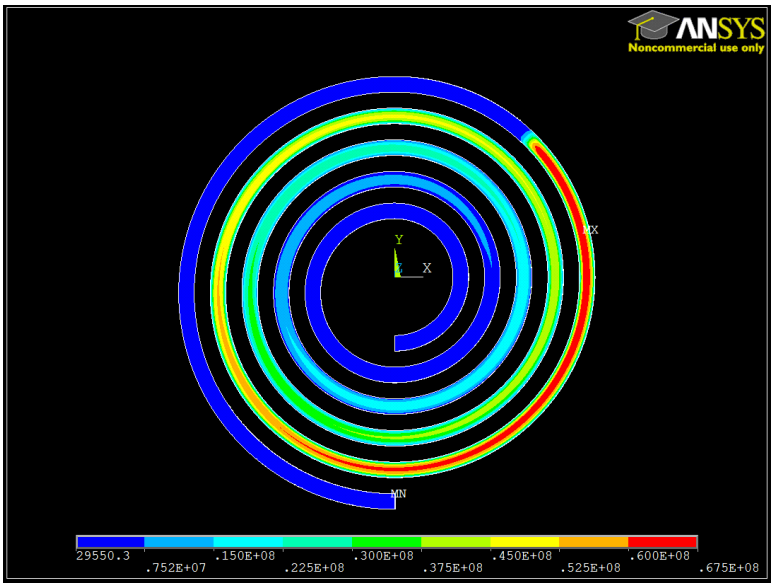

Figure 15: Contour plot of stress profile for the P-MSM spiral piezoelectric beam.

The highest voltage output occurs at the maximum deflection of the beam and for this reason a strain contour plot is shown in Figure 16. The voltage out of the piezoelectric beam from the simulation is shown in Figure 17.

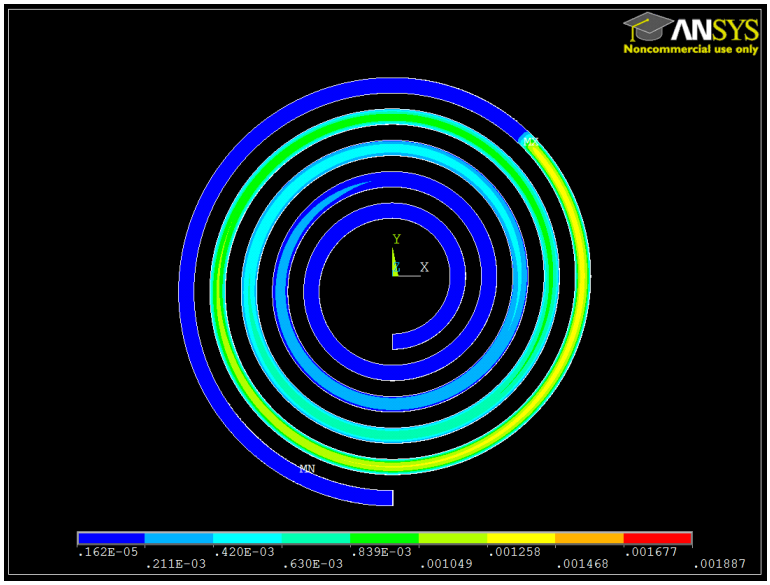

Figure 16: Contour plot of the strain profile for the P-MSM spiral piezoelectric beam.

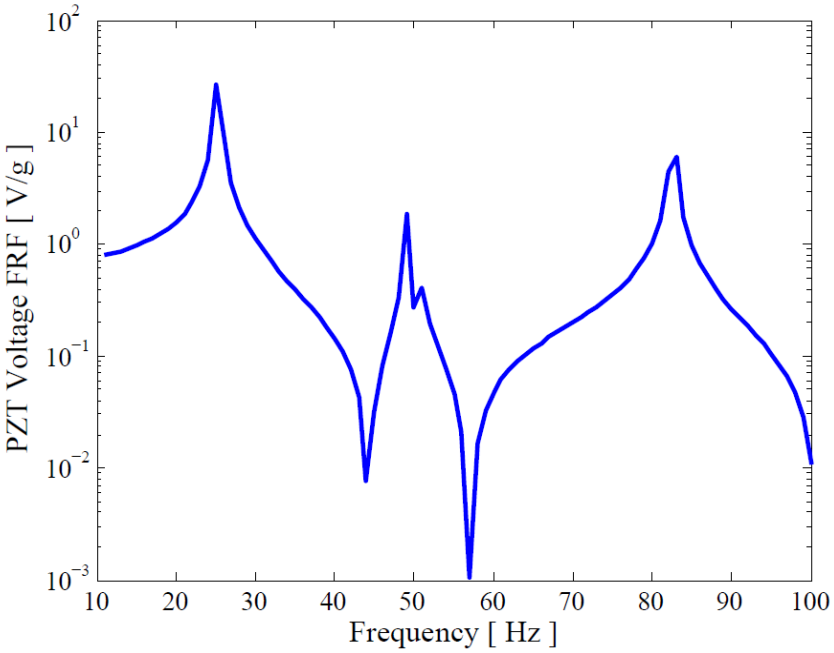

Figure 17: Voltage output from the piezoelectric spiral beam.

The piezoelectric bimorph is wired in an open circuit configuration. The maximum voltage is attained at the maximum strain which occurs at the resonance. As depicted in Figure 17, there are three distinct voltage peaks with each one representing a mode of the system. The first mode is the most prominent mode with the highest effective amplitude and will be one of the main design attributes of this harvester.

4.2.2 Magnetostrictive Model

The magnetostrictive laminates were not modeled due to the extremely nonlinear behavior of the coupling. Furthermore, connecting 100 layers would greatly complicate the simulation. For these reasons only experimental analysis was conducted.

4.3 P-MAG

The P-MAG harvester has both piezoelectric and electromagnetic materials. Due to the nature of the FEA software that was used, both components were modelled separately. The piezoelectric component was modelled on ANSYS, in a similar manner as the P-MSM, while the electromagnetic part was modelled in COMSOL.

4.3.1 Piezoelectric Model

The piezoelectric material was modelled in ANSYS Mechanical APDL 14.0. It was setup in the same way as the P-MSM harvester with the exception of adding the magnet to the bottom of the spiral (Refer to Figure 18).

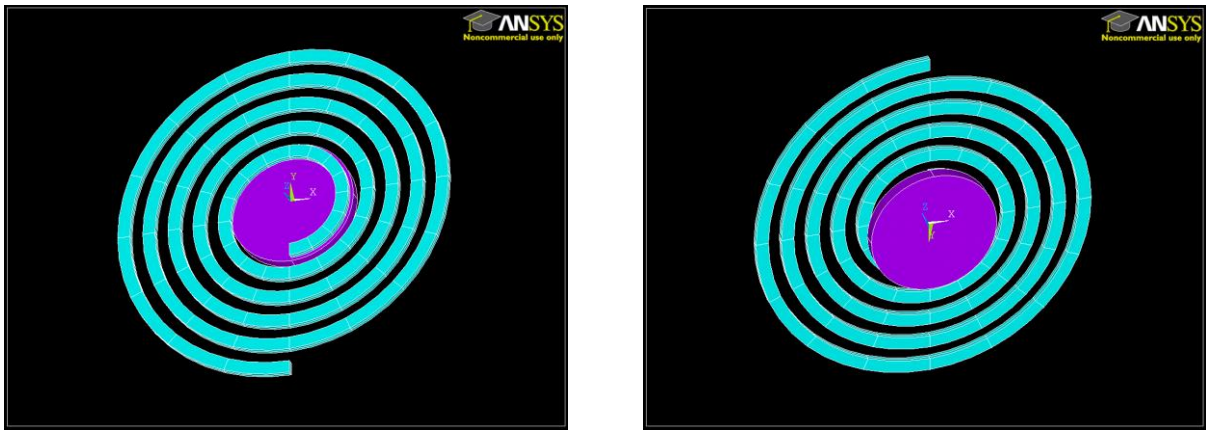

(a) Top view (b) Bottom view

Figure 18: P-MAG harvester (a) from a top view and (b) from a bottom view.

In the ANSYS simulation the magnet was simply added for its mechanical effect on the piezoelectric material and did not possess any magnetic properties; it was simply added as dead weight by specifying its dimensions and density. Table 4 shows the difference in setting up the two materials for the simulation. They both have a different element types due to the fact that the magnet is not a coupled material and is acting simply as added mass.

Table 4: Properties of P-MAG on ANSYS.

	Piezoelectric	**Magnet**
Element Type	Solid 226	Solid 186
Number of Elements	12,320	3825
Volume	763.41 mm^3	78.6 mm^3

Similar to the P-MSM harvester, the stresses in the piezoelectric beam must be tested in order to ensure that the added weight of the magnet does not cause any cracks or failure in the beam. Figure 19 shows the areas with the maximum and minimum stress and as observed from the ANSYS simulation they are well below the tolerance so the beam will not break or crack.

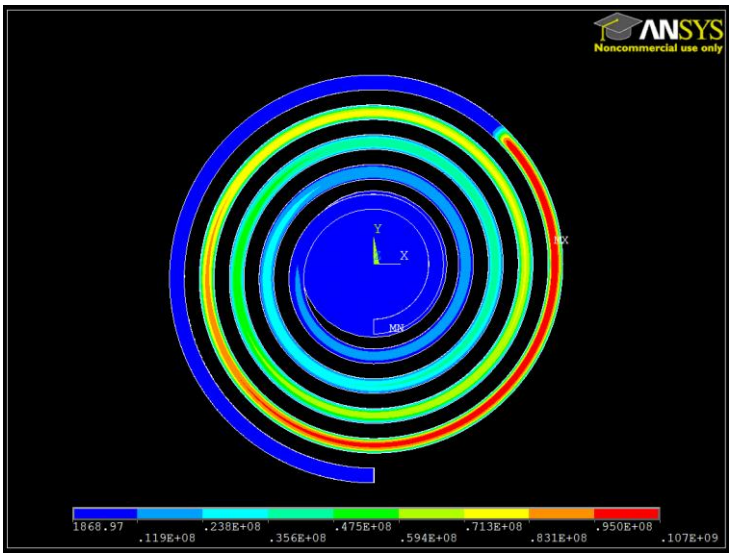

Figure 19: Contour plot of the stress profile for the P-MAG piezoelectric spiral beam.

Similar to the P-MSM simulation, the centre of the spiral is where the displacement sensing takes place. Figure 20 shows the result of the tip displacement of the beam. The first resonance in this case happens at 23 Hz as opposed to the P-MSM spiral beam which was at 25 Hz. This decrease is expected due to the added mass of the magnet where the natural frequencies of a system are inversely proportional to the tip mass.

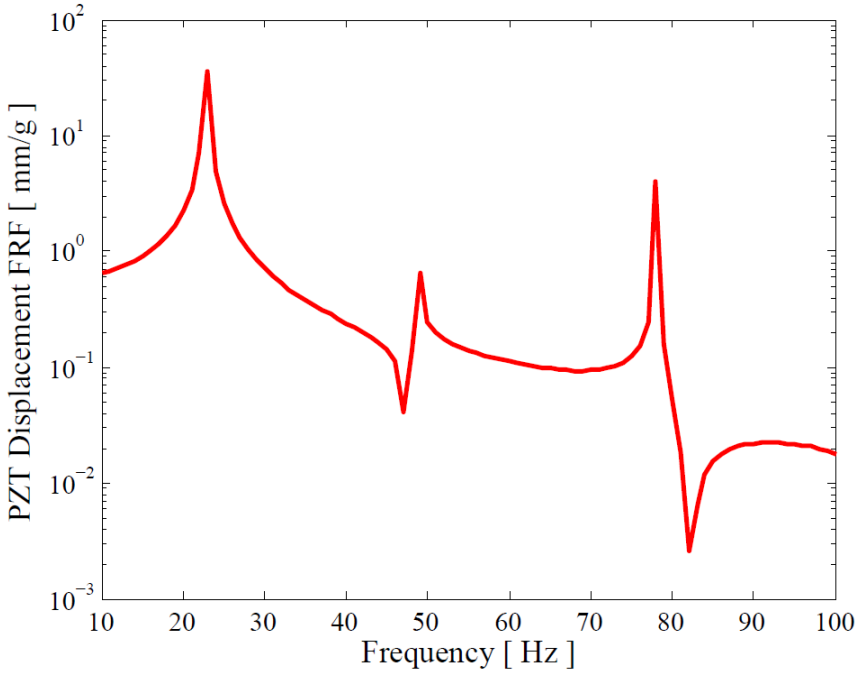

Figure 20: P-MAG tip displacement.

The highest voltage output occurs at the maximum deflection of the beam and for this reason a strain contour plot is shown in Figure 21. The voltage output of the piezoelectric beam from the simulation is shown in Figure 22.

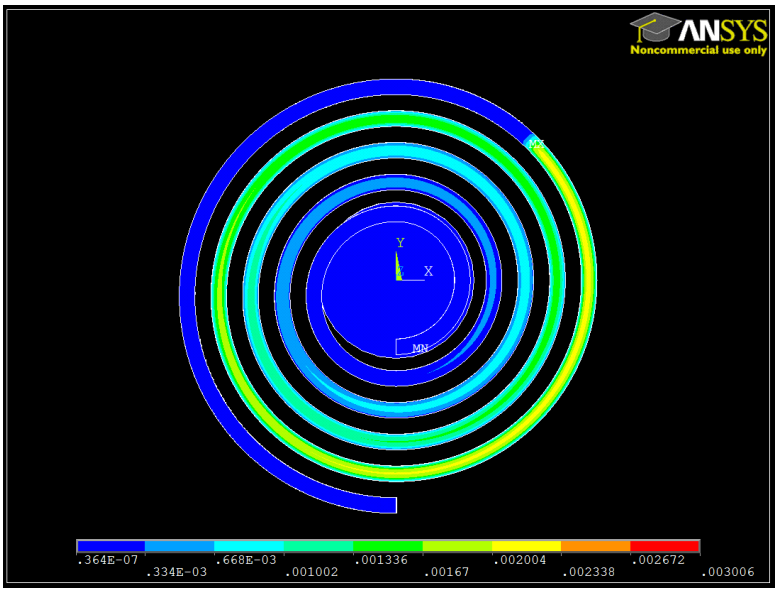

Figure 21: Contour plot of the strain profile for the P-MAG piezoelectric spiral beam.

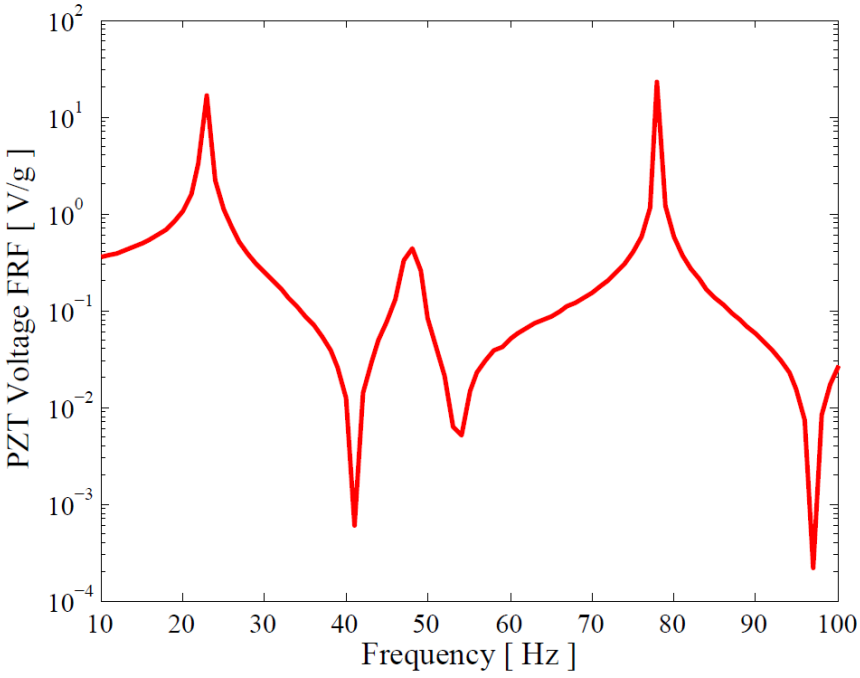

Figure 22: P-MAG voltage output.

The piezoelectric bimorph of the P-MAG harvester is wired in an open circuit configuration as was done for the P-MSM harvester. Due to the nature of piezoelectric material the maximum voltage is attained at

the maximum strain which happens at the resonance. Figure 22 shows the voltage output of the P-MAG to be very similar in shape as that of the P-MSM. Since one of the goals of this thesis is to harvest energy at low frequencies the first resonance will be the main focus.

4.3.2 Magnet

Another FEA was created to model the magnet of the P-MAG harvester. COMSOL Multiphysics 4.3b was used due to its superior electromagnetic capabilities compared to ANSYS. A 2-dimensional axisymmetric analysis was performed using the "Magnetic Fields" and "Moving Mesh" solvers. Figure 23 depicts the geometry that was designed on COMSOL. There is a magnet that moves in the vertical direction and a stationary multi turn coil, surrounded by air. Through Faraday's law of induction, a voltage is induced in the stationary coil from the motion of the magnet.

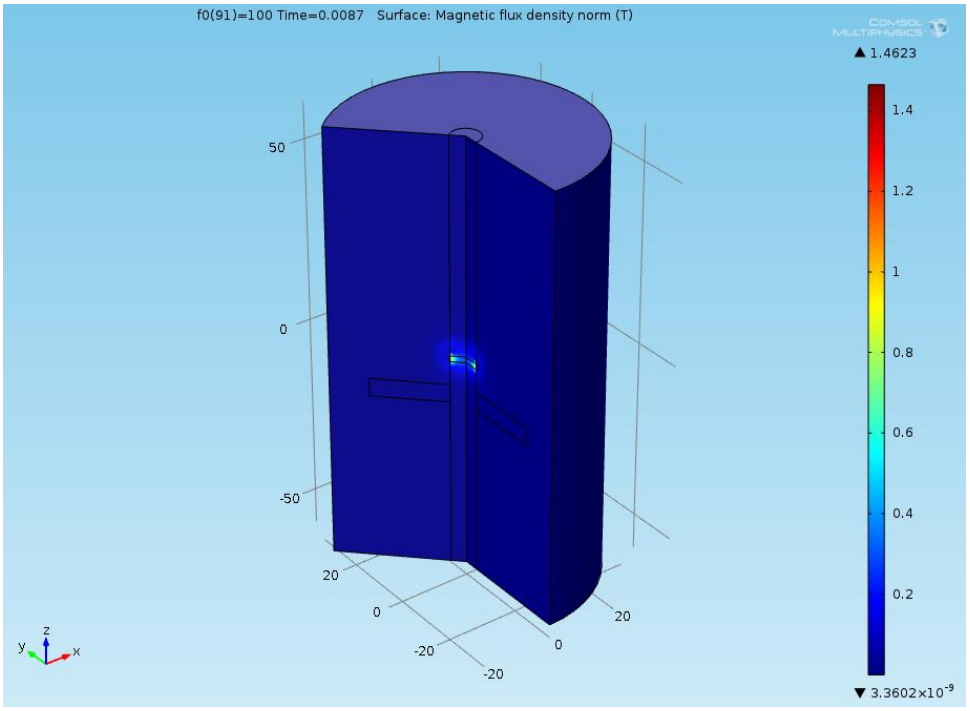

Figure 23: 3-D COMSOL geometry and magnetic flux results.

This geometry was then meshed with 479 triangular elements. The values of the properties that where inputted in COMSOL are given in Table 5.

Table 5: COMSOL simulation values.

Property	Value
Magnetic Flux	1.48 T
Multi Turn Coil	500 Turns
Coil Material	Copper
Wire Gauge	38 AWG

To properly model the magnetic field around the magnet and coil, the air around the magnet and the coil must also be modelled and meshed in COMSOL. The magnet's motion is directly inputted into COMSOL from the ANSYS simulation in order to simplify the model. The air directly above and below the magnet is modelled as a moving mesh due to the fact that the magnet moves and the mesh must move around to accommodate this motion. Refer to Figure 23 for the 3-dimensional contour plot of the magnetic flux density of the model. This figure shows the magnet moving through a multi-turn coil surrounded by air, which represents the actual system.

Figure 24 shows the voltage output of the copper coil which is directly related to the motion of the magnet. The motion of the magnet is taken from the motion of the center of the spiral piezoelectric beam. For that reason the natural frequencies of this graph match perfectly with those in Figure 20. They are one system that is mechanically connected and expected to have the same resonance frequency.

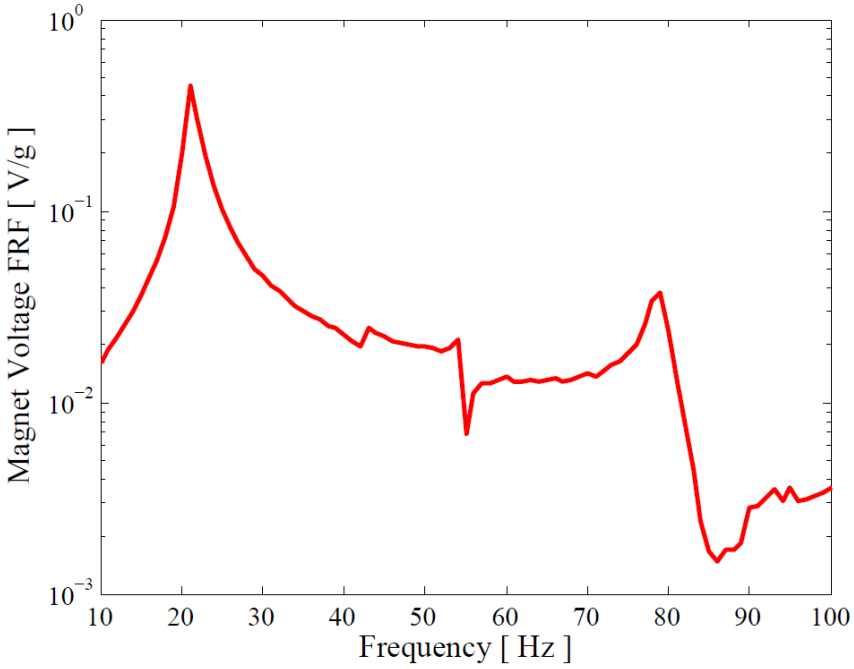

Figure 24: Voltage results for the magnet.

Chapter 5: Experimental Procedures

This chapter describes in detail the experimental procedures. Discussed in this chapter are the steps taken to perform the experiments as well as the building and design of the prototypes for the two harvesters. The different equipment and measuring devices used are outlined. Lastly, the chapter presents the results of the experiments which will appear in the proceedings of AMMCS 2013.

5.1 Material Fabrication

Due to the complex nature of the design geometry, further research was needed to determine an appropriate fabrication method. This was a necessary step before any reliable testing could begin. Conventional and non-conventional fabrication methods were tested in order to realize the spiral design geometry that was intended.

5.1.1 Piezoelectric Material

Piezoelectric material has many different composites that are designed specifically for sensing, actuating, and harvesting applications. As mentioned in Chapter 2, the piezoelectric material with the highest coupling is PZT. There are different types within this material as is listed in Table 3. Type 5H has a higher coupling than type 5A, but only can only be produced in thickness less than 0.25 mm. For that reason the testing done in this work used piezoelectric type 5A (PSI-5A4E). The material was purchased from Piezo Systems Inc. located in Massachusetts and is produced in 0.5 mm thick plates [45].

Machining

A common method to manufacture piezoelectric material is regular machining. The piezoelectric material can be successfully cut in straight lines using this method by using a diamond drill bit (depicted in Figure 25). When the same method was applied to the spiral geometry the piezoelectric plate would often break, due to the relatively small arcs that form the spiral shape. This method proved ineffective for cutting the spiral shape geometry.

Figure 25: Diamond drill bit.

Laser machining

Laser machining using a carbon dioxide laser (CO_2 laser) was tested as a method to cut piezoelectric material. The laser used is a Universal Laser Systems VLS 2.30 desktop laser. The benefit of a CO_2 laser is that it works well on non-metal materials. This laser was successful in cutting piezoelectric material that was less than $0.125\,mm$ thick. Any additional increase in thickness caused unreliable cutting and failure to consistently penetrate through the entirety of the piezoelectric material.

Some of the observations made were that the piezoelectric material heats up to a point where discoloration begins. Figure 26 depicts a small 1x1 mm square that was cut from a plate using this method. From this figure it is clear that the cut did not result in smooth edges and the pieces were red in color, giving a burnt appearance. This could be attributed to the laser power being too high and thus creating too much heat.

Figure 26: A square that was laser machined from the piezoelectric material using high power settings.

To avoid discoloration and possible loss of piezoelectric coupling properties through depolarization, the power of the laser was decreased with the aim of attaining a smooth cut. As depicted in Figure 27 the edges became orange in color and the cut did not fully penetrate the material. The cut made at the edges is also very rough and excess heat remained an issue.

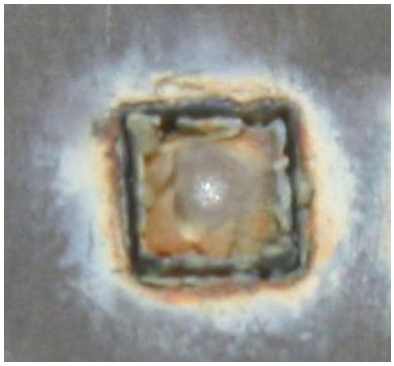

Figure 27: A square that was laser machined from the piezoelectric material using low power settings.

For this reason a Neodymium-Doped Yttrium Aluminum Garnet laser (Nd:YAG laser) machine was then tested. This laser has a shorter cutting time than the CO_2 laser but is used mainly for cutting metals. The reasoning behind using this machine is due to the speed of the laser beam. The idea is that if the beam is faster then it would not stay on the same area for a prolonged period of time and hopefully this would reduce the heat that the material experiences, decreasing the chances of depolarization. The Nd:YAG laser, unfortunately, gave very similar results to the CO_2 laser and was unsuccessful at cutting the material.

Water Jet

A water jet was used after the laser machining failed to cut the thick 0.5 mm piezoelectric sheet. The water jet method uses highly pressurized water that is shot through a fine tipped nozzle attached on a robotic arm that controls its motion in the x and y planes. The nozzle heads change depending on the thickness of the stream of water which then relates to the thickness of the cut. Although water jetting seems like a very aggressive method it proved to be successful. Figure 28 below shows the final piezoelectric spiral beam after it was cut. To ensure there were no micro cracks in the material, it was observed under a microscope. Figure 29 shows a sample of the pictures taken by the microscope at the edges of the piezoelectric spiral. The piezoelectric spiral has an overall mass of 4.95 g.

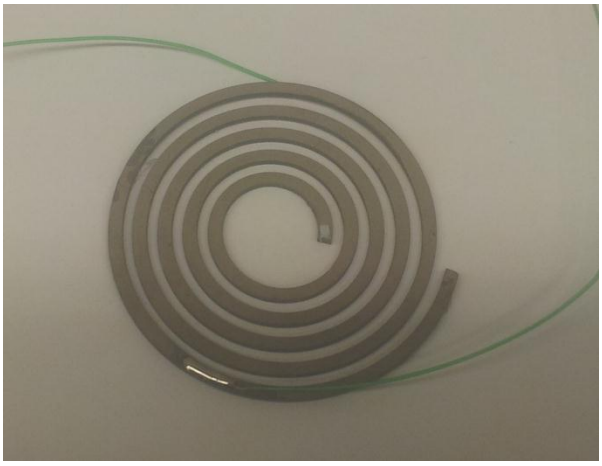

Figure 28: Final cut of the piezoelectric bimorph.

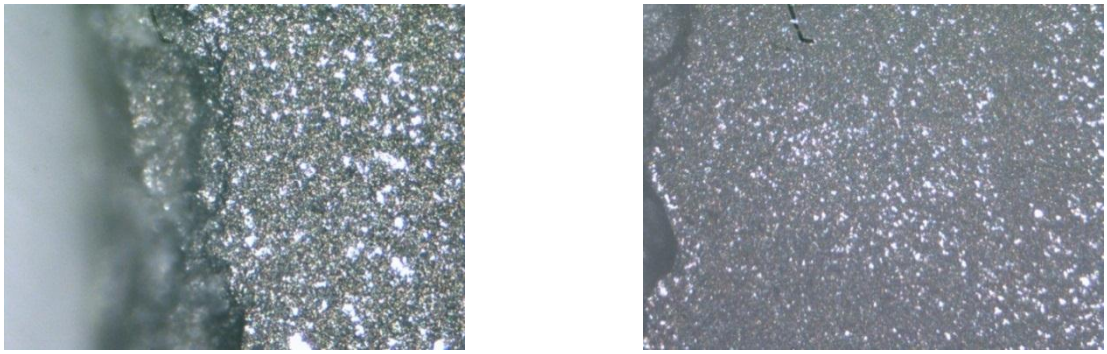

Figure 29: Microscopic pictures of the piezoelectric material after water jet.

5.1.2 MSM

The magnetostrictive material (MSM) that was used is Metglas Magnetic Alloy 2605-SA1, purchased from Metglas Incorporated [46]. This material was chosen due its high permeability and low magnetic losses at lower frequencies, which is one of the design features for the harvester. This material comes in standard 25 μm thick laminates making the effect of a single layer negligible. For that reason, and to increase the overall effect, multiple layers were used in conjunction. Different methods where explored to try and cut this material into a spiral shape.

Laser Machining

Similar to piezoelectric material, the CO_2 laser was also tested to cut the magnetostrictive material. As stated above the MSM comes in very thin laminate sheets, which give it a look almost like aluminium foil. As soon as the laser beam hits the material it immediately starts wrinkling and deforms. This causes

an uneven level for the laser to cut and the material is moved from the focal point of the beam. The result is a partially cut wrinkled part. Laser machining was not successful for this material.

Electric Discharge Machining

Electric Discharge Machining (EDM) is a machining method that cuts the material by controlling an electric discharge, which is a spark that is created between two electrodes by applying a voltage on either side. One of the electrodes is a tip that is controlled by the machine and the other electrode is the material being cut. For this reason EDM can only be used on conductive material.

Since multiple MSM layers would be needed to produce a stronger magnetic effect and reasonable harvesting capability, it was necessary to create a stack of multiple layers. In this work, 100 MSM layers were sandwiched between two pieces of steel that were then tightly clamped together. This was done due to the nature of the MSM to wrinkle and deform. It also keeps all the MSM layers in line with each other in order to have a consistent cut through all the layers. This method was successful in cutting MSM, and the result was 100 layers of spiral shapes pieces that have a mass of 10.27 g.

Annealing

MSM is a ferromagnetic material meaning it has magnetic dipoles that are fixed. Generally, a bias magnetic field is applied to this material to align the magnetic dipoles in one direction. To further increase the magnetic effect, the magnetic dipoles can be aligned through annealing and then a bias magnetic field applied. Depicted in Figure 30 is the field annealed versus the no-field annealed properties of this specific MSM [47]. In both cases, the material is annealed, but one has an external magnetic field during the annealing process. From the figure there is a clear advantage to annealing while applying a field as it allows the MSM to have a stronger magnetic field even when the external field is removed.

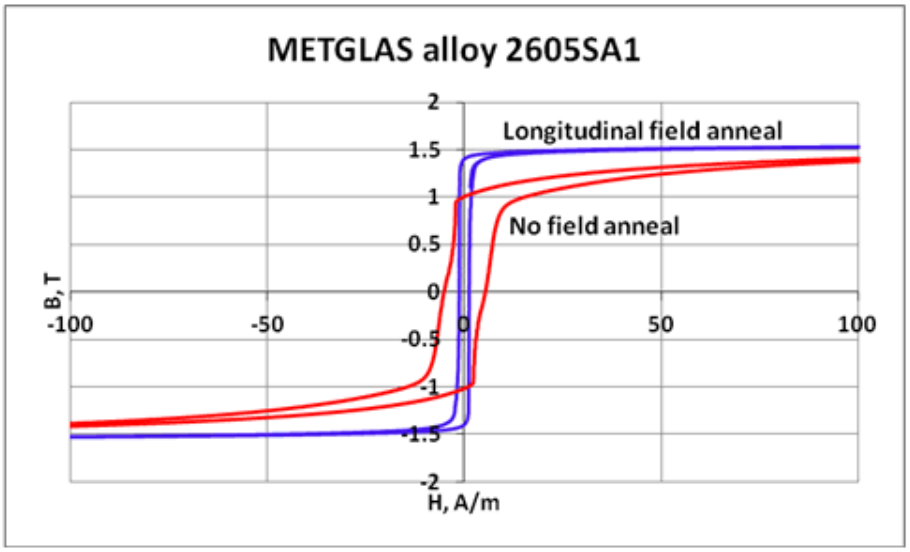

Figure 30: Metglas 2605 SA1 field annealed vs. no field annealed [47].

Figure 31 illustrates the steps that ferromagnetic materials undergo when they are being annealed. Initially the magnetic dipoles in the material are fixed and un-aligned (refer to Figure 31a). The material was then placed in an oven and subjected to heat. As it is heated the membrane around the magnetic dipole starts to weaken (Figure 31b). When it reaches a specific temperature the magnetic dipoles become free to move in any direction (Figure 31c). This temperature is known as the Curie temperature. When ferromagnetic material is heated to a temperature surpassing its Curie temperature, they act like a paramagnetic material. This means that their internal magnetic dipoles are free to move and are influenced by the environment to which they are subjected. An external magnetic field is then applied (Figure 31d) and the magnetic dipoles of the material align themselves with the external field (Figure 31e). The material is then cooled in order to rebuild the membrane that surrounds the dipoles and keep them in place (Figure 31f).

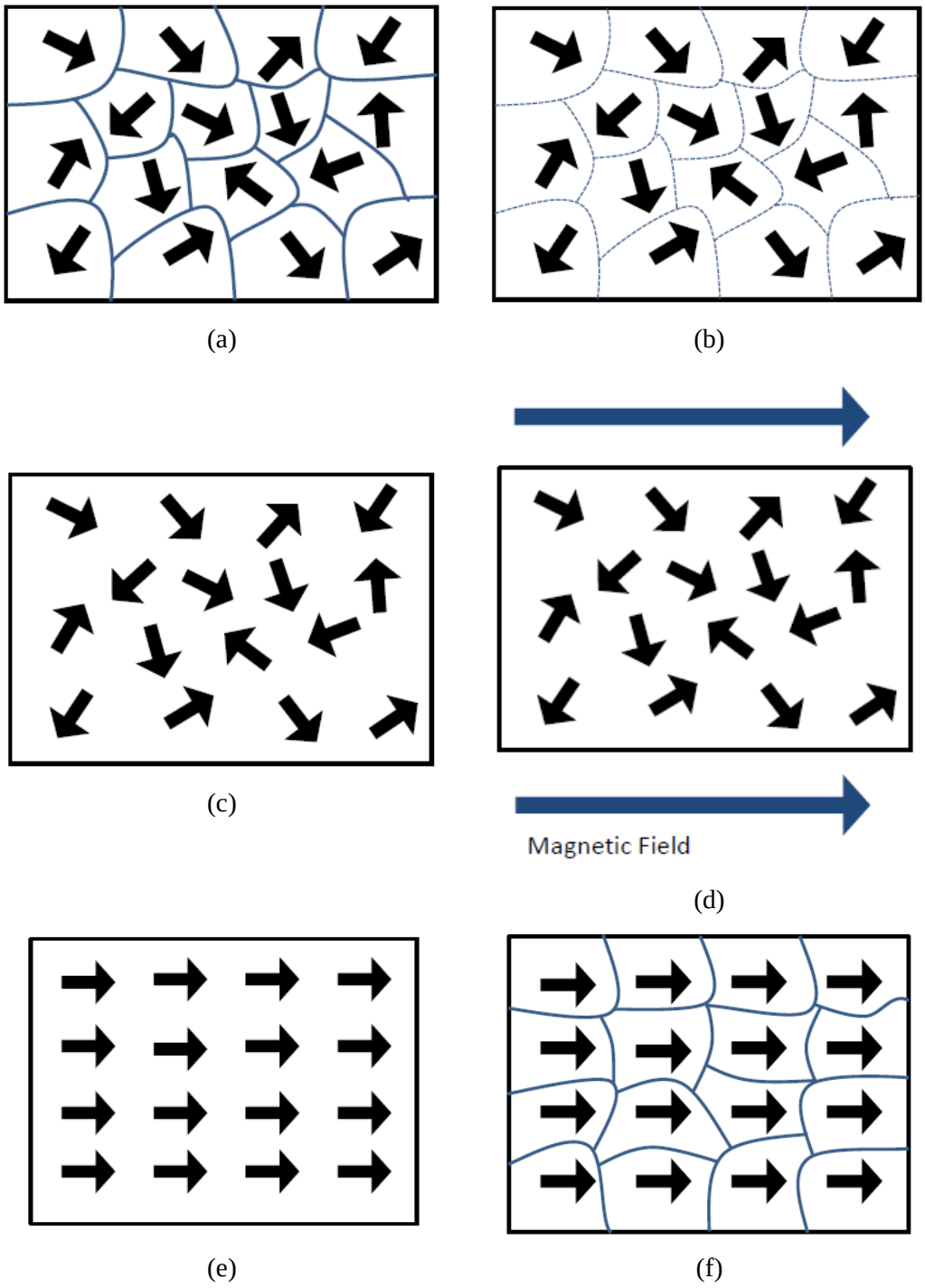

Figure 31: Explanation of the annealing of the magnetostrictive material.

For this MSM material two high temperature magnets were used to apply the external magnetic field during annealing. They supplied 1500 Gauss through the thickness of the spiral, which was applied throughout the entire heating and cooling cycle. Depicted in Figure 32 is the Lindberg/Blue M box furnace that was used for annealing.

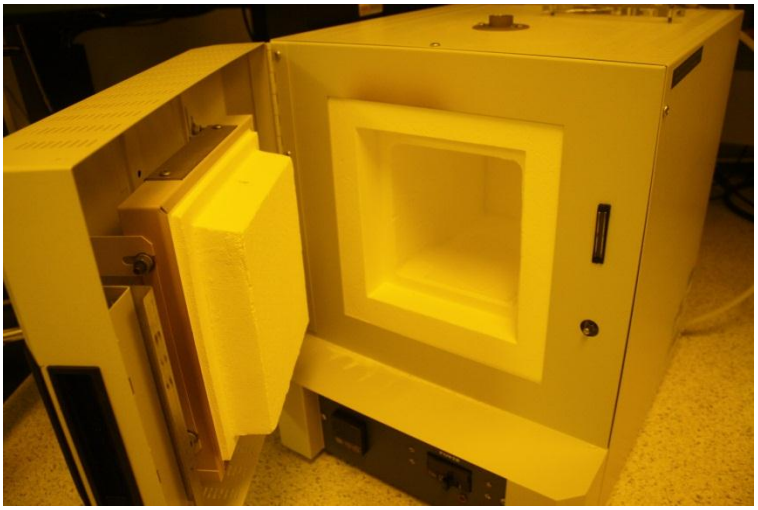

Figure 32: Lindberg/Blue M box furnace used for annealing MSM.

The oven was set following the temperature profile shown in Figure 33 that corresponds to the annealing steps that were previously explained. As depicted in the figure the oven went from room temperature to 450 ºC in one hour. The Curie temperature of the MSM is 425 ºC. It then stayed at this temperature for 3 hours to allow ample time for the material's dipoles to align with the external field. After that it cools down to room temperature once again in one hour. The temperatures and durations used were specified by Metglas Incorporated.

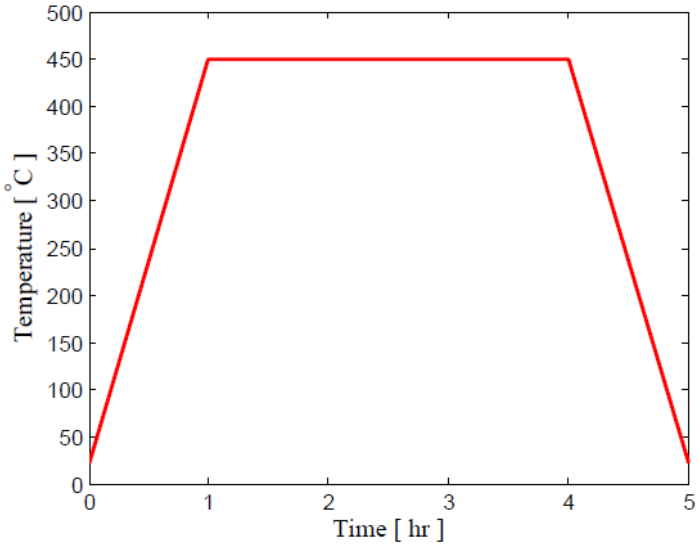

Figure 33: Oven temperature profile for annealing.

5.1.3 Magnets

As discussed in the Chapter 2, magnets are very common in energy harvesting applications. Through Faraday's law of induction a voltage can be produced in a coil if it is exposed to a changing magnetic field, i.e. a moving magnet. A type of rare earth magnet that is commonly used in harvesting application is Neodymium magnets (NdFeB magnets) as they are among the strongest permanent magnets that can be made.

Attaching a magnet in the middle of the piezoelectric spiral would allow for two sources of energy. The D51 NdFeB magnet Grade N52 purchased from K&J Magnetics, Inc. [48] is used for this application. It has a diameter of 8 mm and a thickness of 1.6 mm and is axially magnetized with a mass of 0.6 g (Refer to Figure 34). This particular size magnet was chosen so that it would not interfere with the spiral beam during vibrations.

Figure 34: The D51-N52 NdFeB Magnet.

5.2 Circuit

The piezoelectric material as explained in previous sections is wired in a series connection. The output from the top and bottom layer gives the open circuit voltage. For the purposes of this research, the circuit attached to the spiral is simplified to a simple resistive load in order to focus on the energy harvesting aspect.

To obtain the maximum power output for this system the internal resistance of the piezoelectric material, R_I, has to equal the load resistance, R_L. This idea is explained by the Maximum Power Transfer Theorem, and can be seen below.

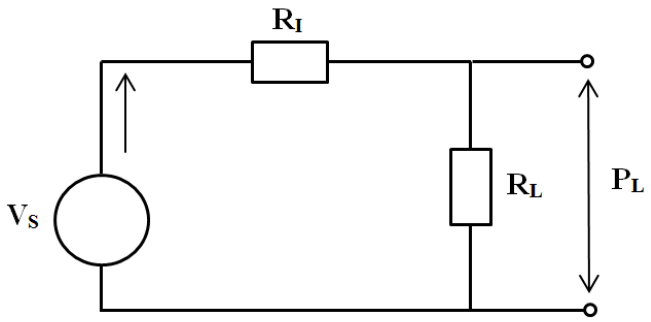

Figure 35: Basic electric circuit.

$$I = \frac{V}{R} = \frac{V}{R_I + R_L} \tag{14}$$

$$P_L = I^2 R_L = \frac{V^2}{R_I^2 + 2R_I R_L + R_L^2} R_L \tag{15}$$

$$P_L = \frac{V^2}{\frac{R_I^2}{R_L} + 2R_I + R_L} \tag{16}$$

In order to maximize the power at the load P_L the denominator of Eq. (16) should be at a minimum. This is performed by taking the derivative of the denominator and equating it to zero.

$$\frac{d}{dR_L}\left(\frac{R_I^2}{R_L} + 2R_I + R_L\right) = 0 \tag{17}$$

$$\frac{-R_I^2}{R_L^2} + 0 + 1 = 0 \tag{18}$$

$$R_I = R_L \tag{19}$$

Eq. (19) shows that that the maximum power at the load occurs when the internal resistance of the piezoelectric spiral is equal to the resistance at the load. The next step is to find the internal resistance of the piezoelectric spiral.

A common method used to determine the resistance of piezoelectric material is to connect a potentiometer at the load of the circuit and run the same acceleration profile sweep while increasing the resistance for each run and recording the power output. Table 6 shows the different resistance values that were used and the corresponding power output.

Table 6: Resistance values with the corresponding power output.

Resistance [$k\Omega$]	Voltage [V]	Power [μW]
1	0.00446305	0.019918817
46.5	0.166227372	0.594226647
100	0.359070202	1.289314102
200	0.578941433	1.675865917
400	0.772703386	1.492676307
1000	0.907405726	0.823385151
1500	0.927730155	0.573788827
2000	0.93846109	0.440354608
3000	0.946104686	0.298371359
5000	0.960426808	0.184483931

These results are plotted in Figure 36 and it is clear there is a peak in the power output at 200 $k\Omega$ load resistance. As per the Maximum Power Transfer Theorem it is concluded that the internal resistance of the piezoelectric spiral is also equal to 200 $k\Omega$.

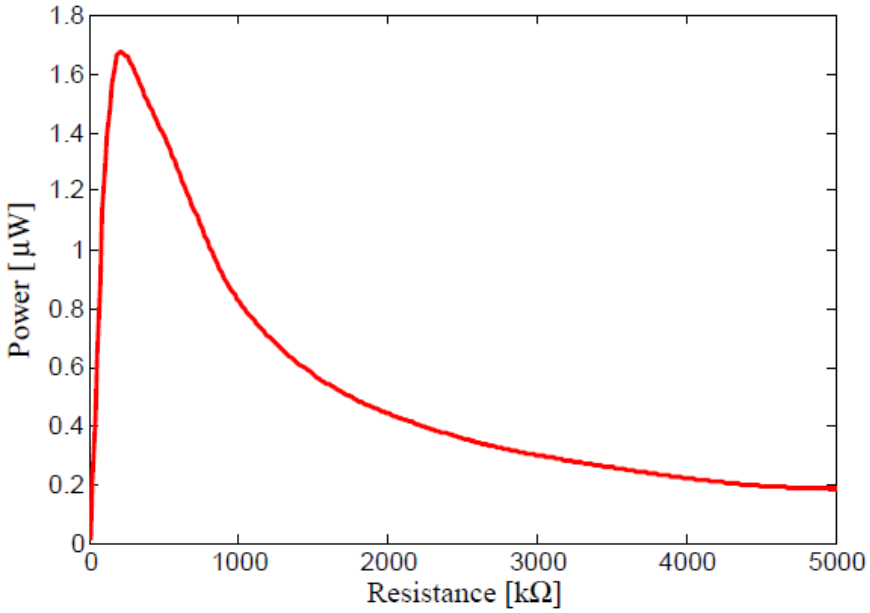

Figure 36: Results of resistance testing of the piezoelectric spiral.

5.3 Testing Setup

After the fabrication of the material, the prototypes needed to be tested in order to determine their performance and efficiency. For the testing to be possible, specific measurement equipment was used. To effectively determine performance of the proposed harvesters they need to be subjected to a known and controlled vibration input and the resulting output voltage or power needs to be recorded.

Figure 37 shows the test setup and the major components used to record the results. As depicted in Figure 37, the setup consists of an electrodynamic shaker, an amplifier, a laser vibrometer, a vibrometer controller, a data acquisition system, and the laptop used for set up and viewing of the data.

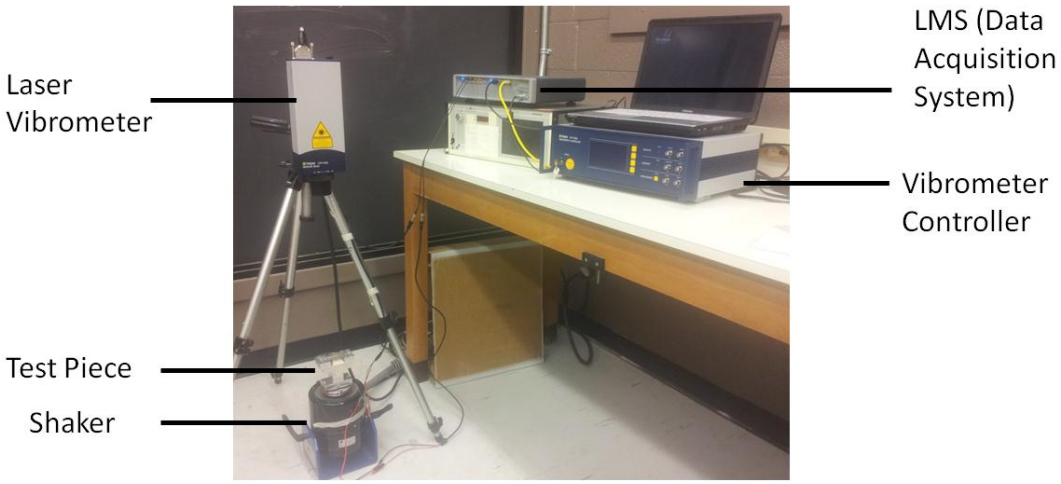

Figure 37: Equipment used and test setup.

A shaker is used as the vibration source for the harvester. It is a Modal Shop 2075E Dual Purpose Shaker. It is a permanent magnet shaker that can provide up to 334 N of force. It has a standard turnnion mounting base that allows for a 90° rotation for different axis excitation. The armature has a stroke of 25.4 mm and can be operated at frequencies up to 6500 Hz.

The shaker is controlled by LMS SCADAS Mobile Data Acquisition System (DAS). It has 8 input ports to record and process data and 2 output ports that regulate signals. It sends a controlled signal to the shaker through the amplifier in order to reach a desired acceleration. The LMS SCADAS controls this signal using a feedback loop and an accelerometer is used to ensure the desired acceleration levels are met.

The accelerometer used is a 352A24 made by PCB Piezotronics. This accelerometer was chosen due to its versatility. Its sensitivity is 100 mV/g and can operate to frequencies up to 10,000 Hz. Another key component in the setup is the laser vibrometer and its controller. The sensor head is a Polytec OFV 505 and the controller is OFV 5000. It is a laser Doppler vibrometer that works on the Doppler principle, which sends a light beam at a vibrating structure and measures the returning beam to determine velocity and displacement. This is used to measure the deflection of the spiral beams due to the input vibration.

A laptop running LMS Test Lab software is connected to the DAS through an Ethernet cable, which allows it to make the appropriate settings to run the test. The Sine Control module in Test Lab was used. The acceleration was at a constant 0.3g while the frequency was swept from 10 Hz to 100 Hz.

The shaker itself has coils inside it, and when a current goes through them the armature will move. This implies that the coils will have a magnetic field as a result of the current flow, which might affect the results of the pick-up coil for the magnet and the MSM. A 500 turn copper coil was placed on the armature of the shaker. It was exposed to the same vibration profile that will be used for the harvesters in order to see the effect of the shaker's magnetic field. The outcome of this test is displayed in Figure 38, which shows that the coil does indeed pick up noise from the shaker, which will add unwanted noise to the results.

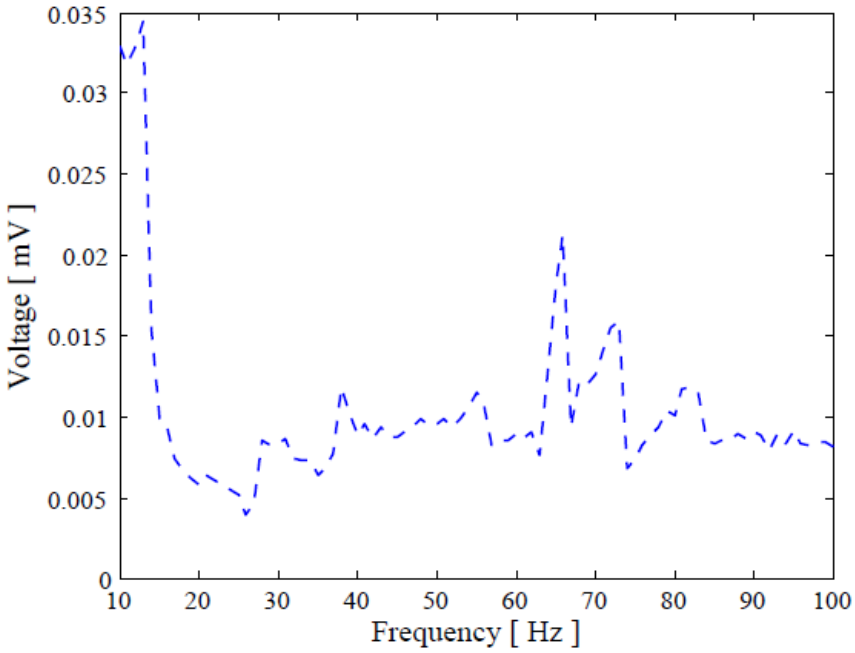

Figure 38: Voltage output from the noise of the shaker.

An aluminum spacer was then fabricated in order to increase the distance between the test piece and the shaker (Refer to Figure 39). The same vibration profile was applied again so see if the noise is reduced. From Figure 40 it is observed that there is around 5 μV of noise from the shaker after being elevated. This indicates that there is less noise and the spacer is sufficient to minimize the magnetic field noise emitted from the shaker.

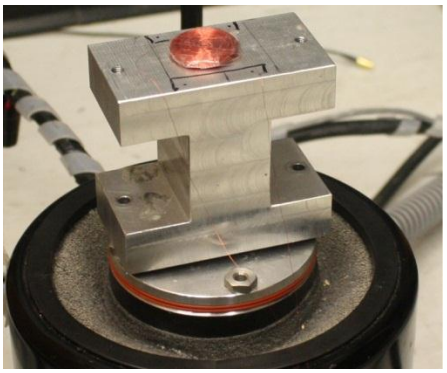

Figure 39: 500 turn coil elevated from the shaker.

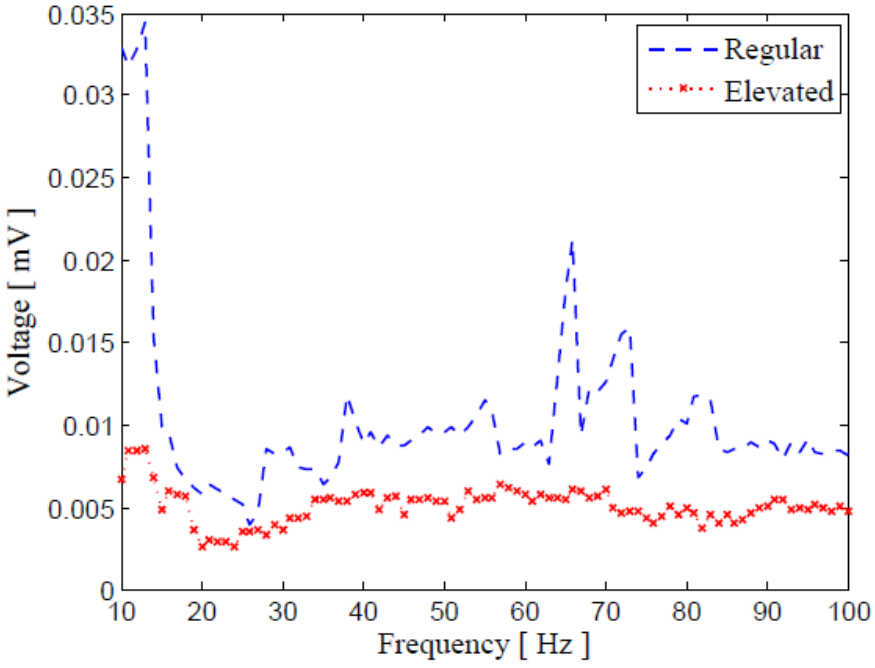

Figure 40: The voltage output of the 500 turn coil elevated from the shaker.

5.4 P-MSM

The first hybrid energy harvester prototype is one that uses piezoelectric and magnetostrictive material, called P-MSM. The idea is to have two different materials with different stiffness coupled together to produce a useful power output.

The fabrication of the piezoelectric spiral and the magnetostrictive spiral was the first step. The next step is the design of a mount that can support both spirals and two, 3000 turn copper coils. Figure 41 shows the mount that was designed to couple all these different elements together. The mount was fabricated through 3-D printing and the material was epoxied into position. Through some experimentation it was

determined that the voltage from the magnetostrictive material was low, and one of the methods to increase the output is to add a bias magnetic field. This bias magnetic field helps align the magnetic poles of the magnetostrictive material. For that reason two magnet channels were added to the mount design to hold small magnets strong enough to create an effective biased magnetic field.

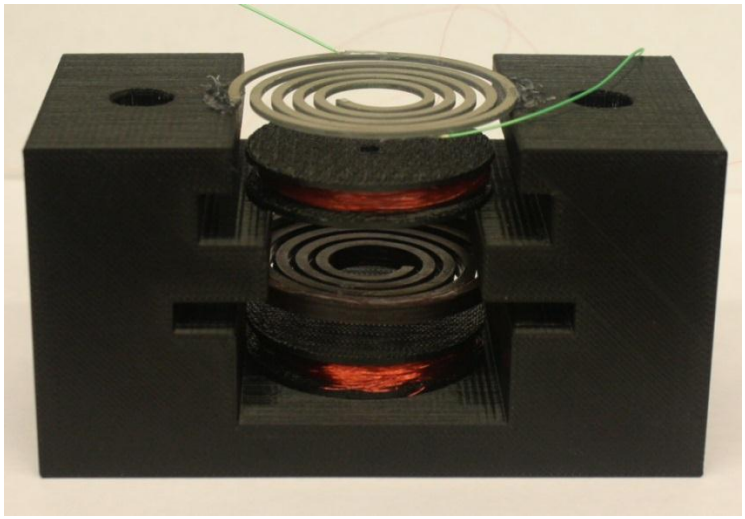

Figure 41: P-MSM Prototype.

Three NdFeB magnets were placed on each side of the magnetostrictive material into the channels located on either side of the mount as can be seen in Figure 41. The field created by these magnets in the area of the magnetostrictive material is depicted in Figure 42. Due to the use of the magnets the magnetic field will not be consistent throughout the length of the material. It will be stronger closer to the magnets and it will weaken at the farthest point from the magnets.

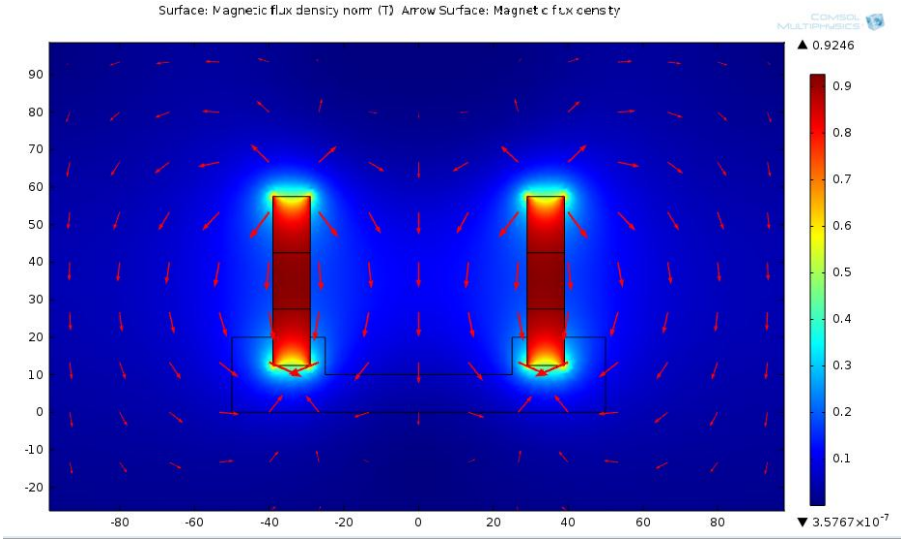

Figure 42: Magnetic field created around the magnetostrictive material.

Figure 43 depicts the bias magnetic field values that the magnetostrictive material experiences. The extents of the spiral go roughly from -20 mm to 20 mm on the x-axis and as shown the field has a maximum at 1500 Oe and the minimum in the centre of the spiral layer at 900 Oe.

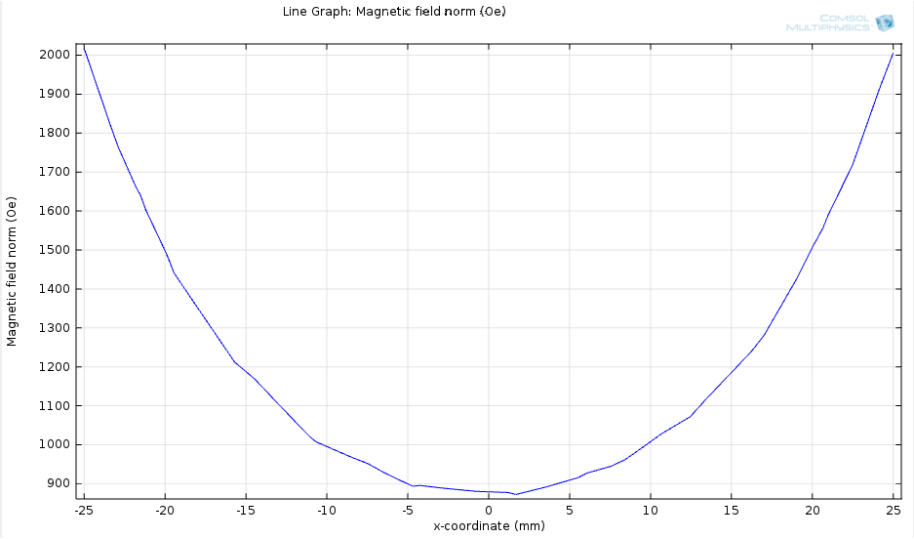

Figure 43: A plot of the value of the bias magnetic field as experienced by the magnetostrictive layer.

The addition of the bias magnet significantly increased the output from the magnetostrictive layer. The unit was then placed on the shaker for vibration testing as explained in previous sections. The power results of both layers where measured separately then they were totalled to obtain the total power this unit can harvest.

Figure 44 and Figure 45 display the frequency response function (FRF) of the displacement and power output of the piezoelectric layer respectively. The displacement is measured at the centre of the spiral (free end) which is measured by the laser vibrometer. The maximum displacement FRF amplitude was 8 mm/g and the maximum power FRF peaked at 20.91 $\mu W/g$. Both these occurred at 23 Hz, which is the first resonant frequency of the piezoelectric material. These results will later be used to make a comparison to the results found in the modelling section.

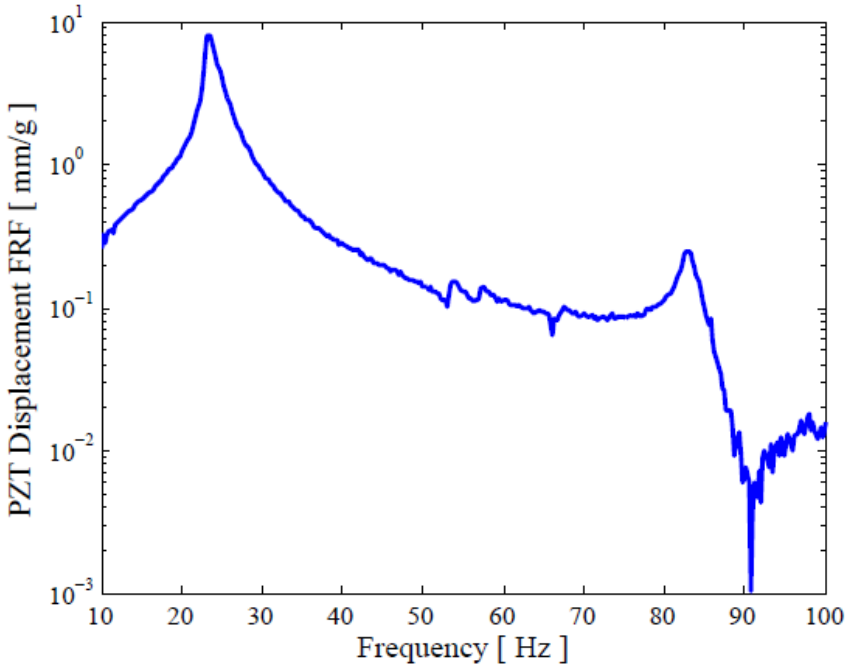

Figure 44: Piezoelectric displacement from the P-MSM harvester.

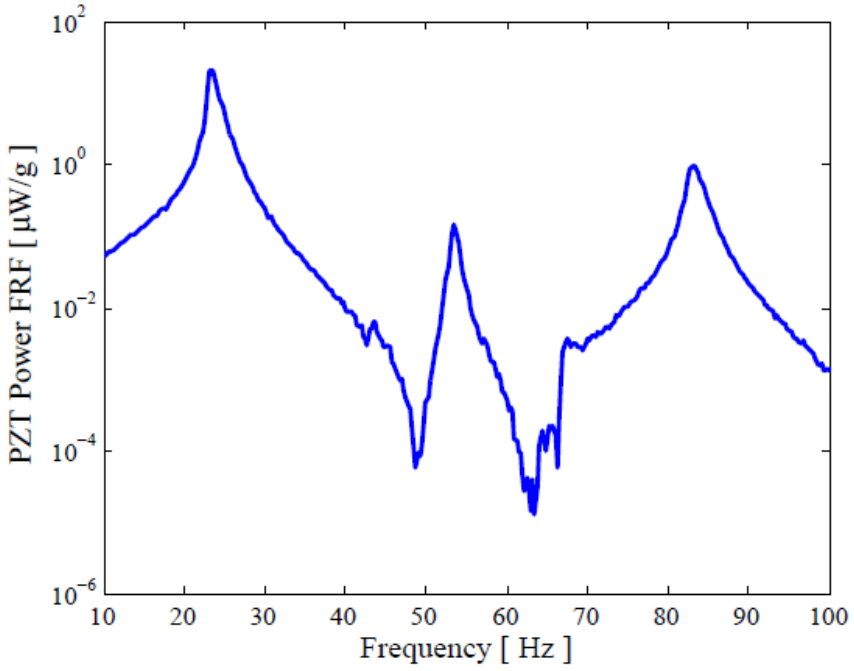

Figure 45: Piezoelectric power from the P-MSM harvester.

Figure 46 displays the power output from the magnetostrictive layer. The peak occurred at a frequency of 17 Hz with an amplitude of 10.07 $\mu W/g$. Figure 47 focuses on the power output at the first natural frequency of the piezoelectric and the magnetostrictive layers. From these results we can conclude that

the two power peaks for the different materials did not occur in the same frequency and had different shapes.

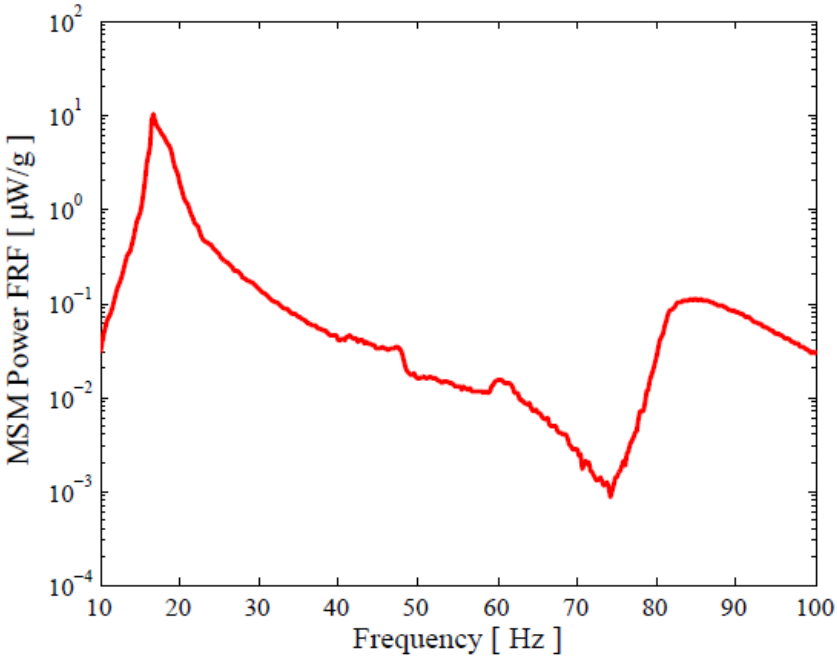

Figure 46: Magnetostrictive power from the P-MSM harvester.

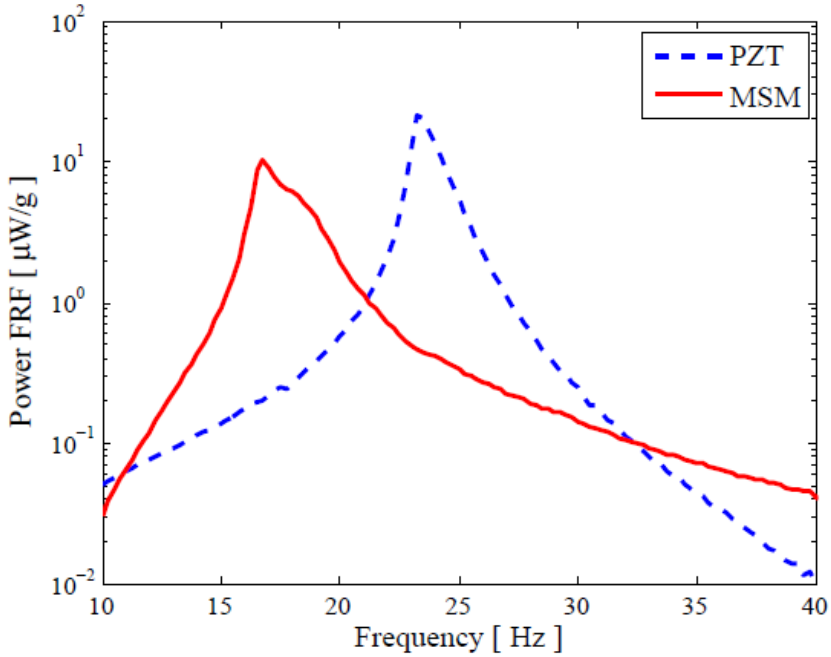

Figure 47: Combined power FRF plots for the piezoelectric and the magnetostrictive layers.

In order to see how the system works as a whole the two power plots will be added together to show the total power FRF for the P-MSM harvester. Figure 48 depicts the power output of the first resonance of each of the materials. In green is the FRF of the overall power output for the harvester. It is observed that the first peak had a value of 10.41 $\mu W/g$ at a frequency of 17 Hz and the second peak had a value of 21.88 $\mu W/g$ at a frequency of 23 Hz.

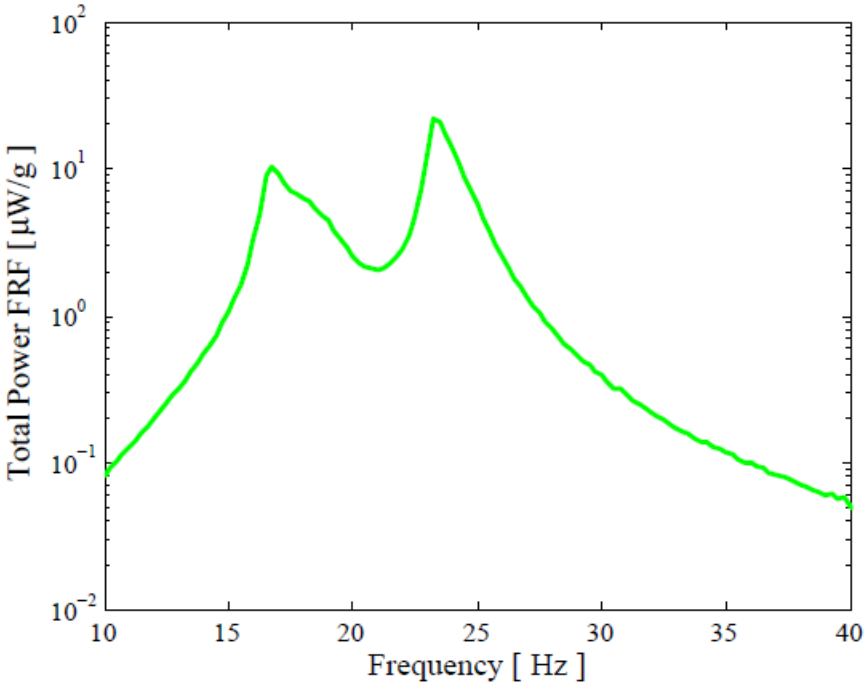

Figure 48: Total power of the P-MSM harvester.

From Figure 48 it is observed that there is a wide band of frequencies that can be used to harvest energy. The lowest power is 2 $\mu W/g$, and the highest power is 21.88 $\mu W/g$. This allows the harvester to be a wide band harvester that can operate for frequencies from 16 Hz to 26 Hz. This is large in comparison to the average range of 1 to 3 Hz for simple energy harvesting that occurs at only one peak. This allows the P-MSM to be advantageous in many applications where the ambient vibration source tends to drift over a range of frequencies.

The average of the power spectral density (PSD) of the PZT from Figure 47 for the frequency range shown (17 Hz to 23 Hz) is 1.97 $\mu W/g$. The PSD for the total power of the hybrid P-MSM harvester in the same frequency range is 5.151 $\mu W/g$, which shows a 160% increase.

5.5 P-MAG

The second hybrid energy harvesting prototype is one that uses piezoelectric and electromagnetic material, called P-MAG. It is formed mainly of piezoelectric material and includes a magnet attached at the centre of the piezoelectric spiral, as shown in Figure 49. Generally, a static mass is used to reduce the natural frequencies of the structure [49]. The benefit of using a magnet in the P-MAG harvester is not only to reduce the frequencies of the system, as would a static mass, but to induce a voltage in a nearby coil. By doing so, the hybrid system produced more power than a simple piezoelectric spiral with only a static mass at a lower frequency.

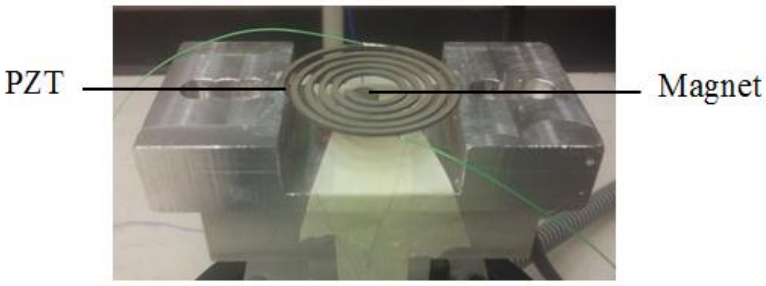

Figure 49: P-MAG Prototype.

Figure 50 and Figure 51 display the FRFs for the displacement and power output of the piezoelectric layer respectively. The displacement is measured at the centre of the spiral where the magnet is also attached. The maximum displacement amplitude was found to be 8.8 mm/g and the maximum power peaked at 18.3 $\mu W/g$. Both of these occurred at 21 Hz, the first resonant frequency of the piezoelectric material. These results will later be compared to the modelling results.

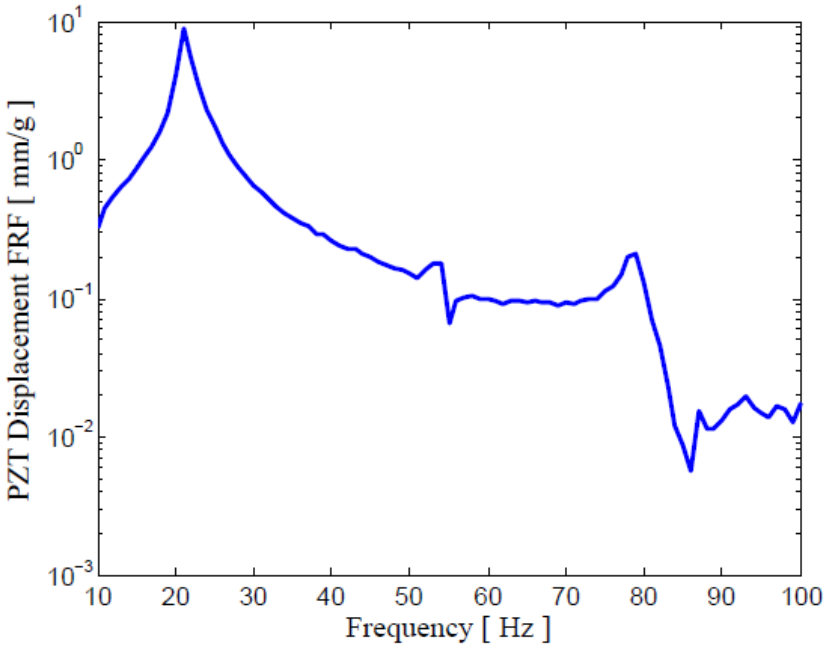

Figure 50: Piezoelectric displacement for P-MAG harvester.

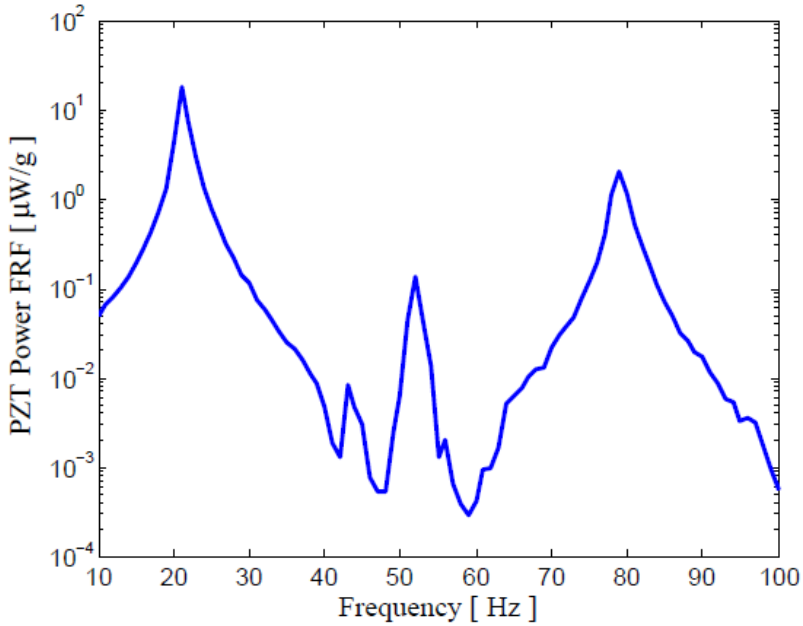

Figure 51: Piezoelectric power for P-MAG harvester.

The magnet will also resonate at 21 Hz because it is attached to the piezoelectric spiral. From the 500 turn copper coil the maximum induced power was 33.79 $\mu W/g$. Figure 53 shows the power of the P-MAG harvester which is found by combining the power output of the magnet and piezoelectric materials. It has

a peak of total power 52 $\mu W/g$ at a frequency of 21 Hz. As expected, the added mass of the magnet reduced the natural frequency of the spiral.

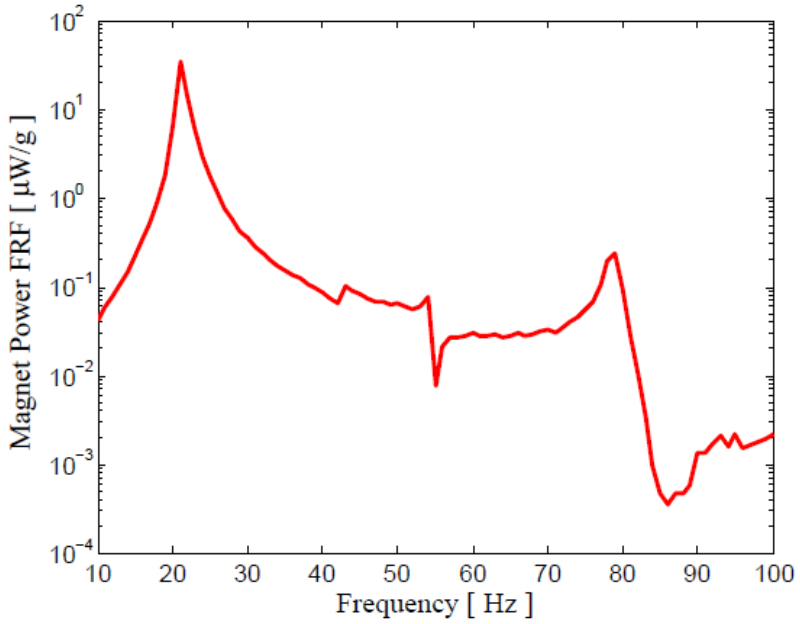

Figure 52: Magnet power for P-MAG harvester.

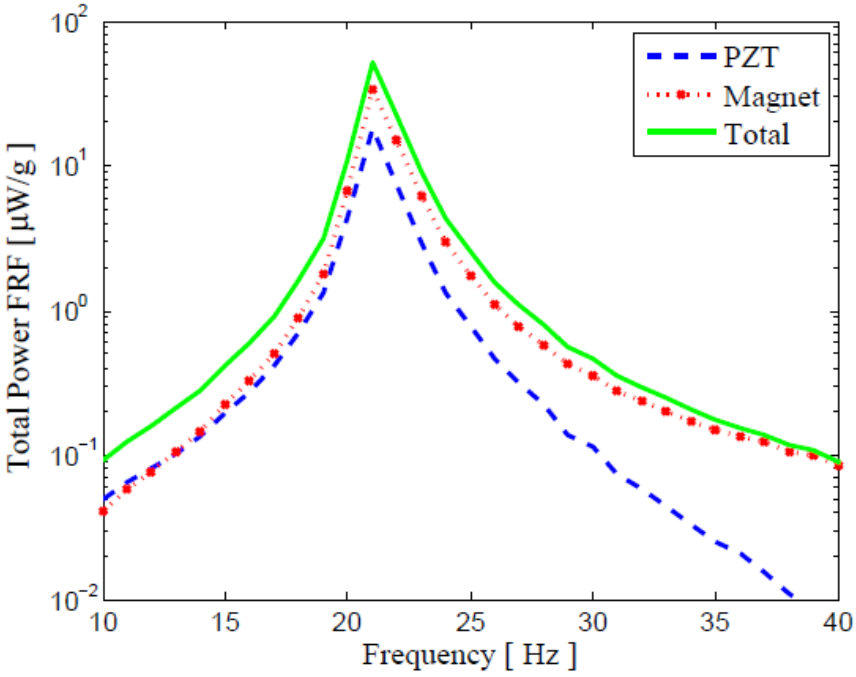

Figure 53: Total power for P-MAG harvester.

Unlike the P-MSM, the P-MAG only had one peak, which means it cannot be used as a wide band harvester. It does however result in higher power output and this, allows the harvester to be used in applications where higher power is necessary.

Chapter 6: Validation and Analysis

This chapter compares the experimental and simulated frequency response functions (FRFs) of each proposed harvester. The validation of the experimental results from Chapter 4 with the simulation results from Chapter 5 is essential to ensure that this system can be modelled appropriately and that the results are repeatable.

6.1 Damping

When the simulation was performed, damping was not considered in the system. Damping exists in any mechanical structure but the value can be small and assumed to be negligible. Damping should be considered in order to get a more accurate model of the system. In this thesis, the quadrature peak picking method outlined in Inman [50] is used to determine the damping ratios from experimental FRFs however many other suitable methods to determine damping ratios exist. The quadrature peak picking method is applicable for lightly damped systems. To obtain the model damping ratio ζ, the displacement FRF of the P-MAG harvester is used as an example (Refer to Figure 54).

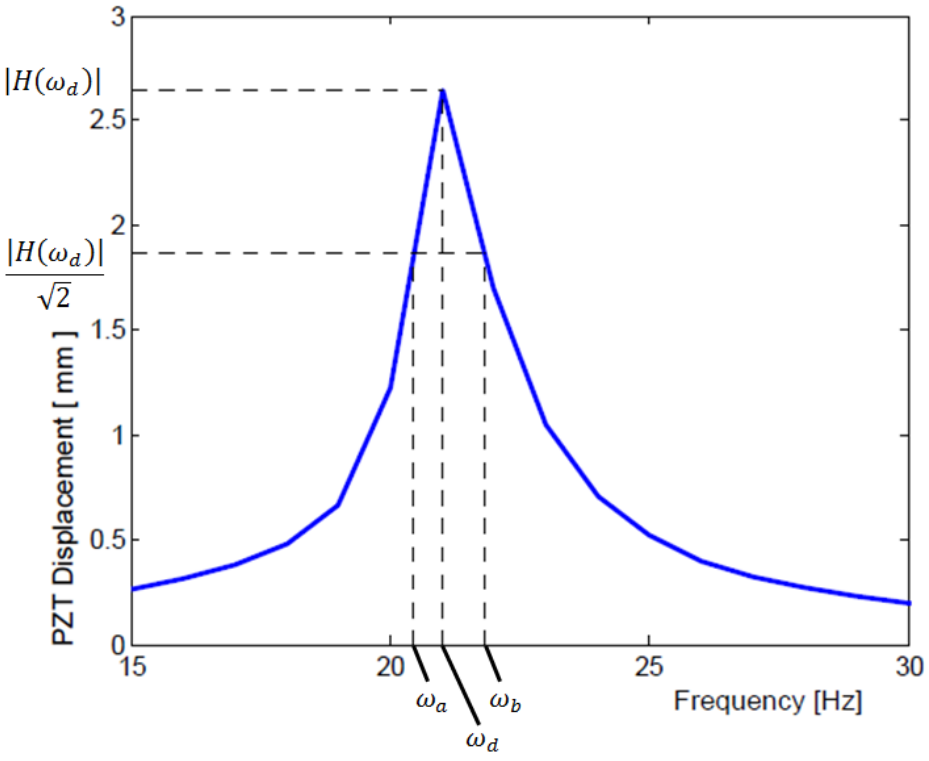

Figure 54: Piezoelectric displacement FRF illustrating the calculation of the damping ratio

From Figure 54, ω_d is the damped natural frequency and $H(\omega_d)/\sqrt{2}$ corresponds to the 3 dB magnitude drop. The relation of ω_a and ω_b to the damping ratio ζ is explained.

$$|H(\omega_a)| = |H(\omega_b)| = \frac{|H(\omega_d)|}{\sqrt{2}} \tag{20}$$

$$\omega_b - \omega_a = 2\zeta\omega_d \tag{21}$$

$$\zeta = \frac{\omega_b - \omega_a}{2\omega_d} \tag{22}$$

Eq. (22) provides the expression to calculate the damping ratio ζ. The ANSYS simulation was previously run without the considering damping. In order to include it ANSYS requires the damping value to be the damping coefficient β.

$$\beta = \frac{2\zeta}{\omega_d} \tag{23}$$

Once the damping coefficient $\beta$of the system is determined, it is used in the ANSYS Mechanical APDL as the damping value for the model. Adding damping to the model will provide a more realistic representation of the experiment that is being performed. Additionally, the results will match more closely with the experiment.

6.2 P-MSM

Recall from Chapter 4 that the piezoelectric layer is the only layer that is modelled in ANSYS for the P-MSM harvester. Figure 55 and Figure 56 show the results of the piezoelectric layer both for displacement of the tip and power output. From Figure 55, it is observed that there is less than a 5% difference for the first peak. The other peak matches closer with the experimental results. This suggests the simulation and the experimental are in good agreement.

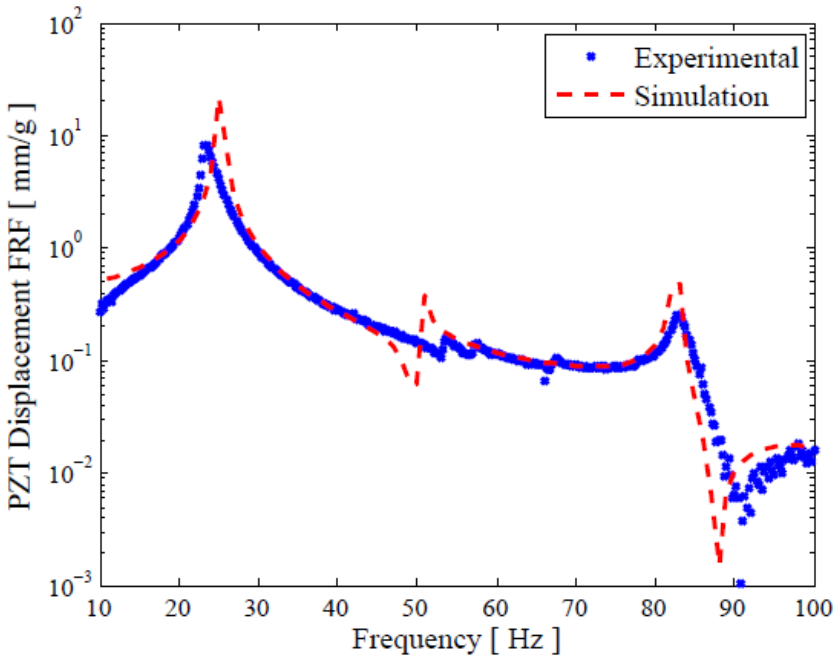

Figure 55: P-MSM results for the experimental vs. the simulation for the tip displacement of the piezoelectric spiral.

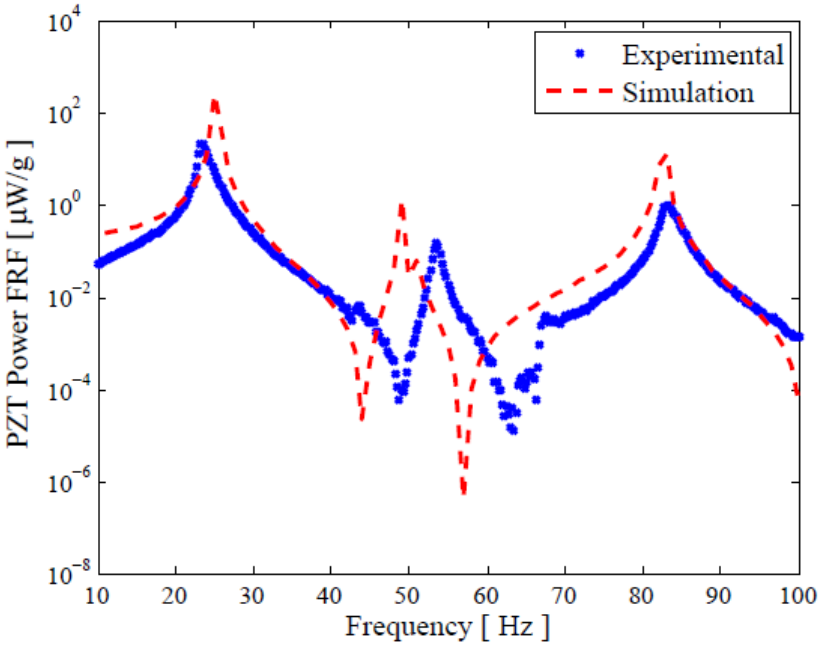

Figure 56: P-MSM results for the experimental vs. the simulation for the power output of the piezoelectric spiral.

Figure 56 depicts the power output of the piezoelectric material. The first peak and third peak are in good agreement with the experimental but the second peak is off by a difference of 9%. To obtain a better

understanding on the how the spiral is moving at the three peaks the mode shapes were animated and the results can be seen in Figure 57.

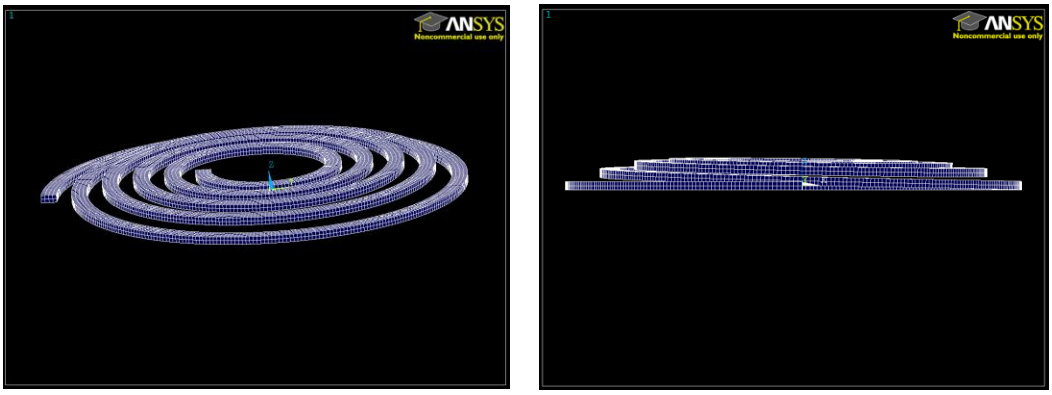

(a)

(b)

(c)

Figure 57: Animating the mode shapes (a) First peak, (b) Second peak, (c) Third peak.

Figure 57a shows the shape of the spiral resonating at 23 Hz, which is the first peak in the FRF. As expected this is the first bending mode of the spiral and the center moves in the same direction as the rest of the surrounding rings. On the other hand, Figure 57b is a torsional mode at 49 Hz. A torsional mode produces strain on the spiral beam but due to torsion rather than bending. This explains why there is a relatively larger second peak in the power plots as opposed to the displacement plots. Torsional modes cannot be detected by sensing the displacement in only one direction, which is what the displacement plots show. The animation of the third peak of the FRF is shown in Figure 57c. This shows that the third peak is the second bending mode of the spiral and also as expected the center of the spiral moves in the opposite direction of the surrounding rings.

Consequently the difference in the second peak of the power plot is explained by the torsional mode at that frequency. For a complex geometry like the spiral the torsional mode shapes are more difficult to model accurately. In this case there is a 9% difference between the experimental and simulation of the torsional mode, which is an acceptable difference due to the geometry.

6.3 P-MAG

The P-MAG harvester has two components, the piezoelectric layer and the attached magnet. The piezoelectric layer displacement and power output modelling in comparison to the experimental is shown in Figure 58 and Figure 59 respectively. It is very similar to the results of the piezoelectric layer in the P-MSM harvester. The results are generally in good agreement except at the second peak, which has an 8% difference in this case. This is explained by the torsional mode at 48 Hz, which is an acceptable difference due to the complex geometry of the spiral.

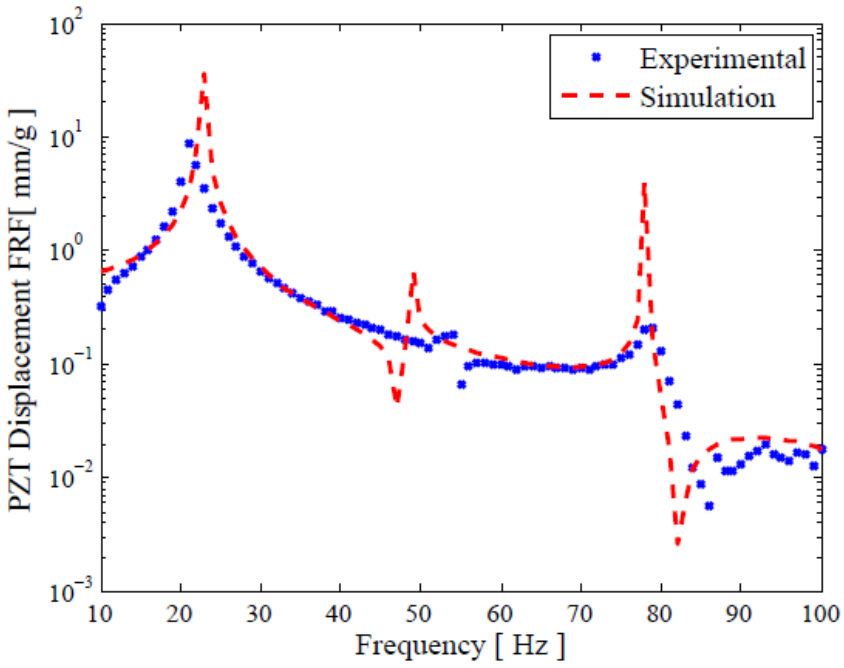

Figure 58: P-MAG results for the experimental vs. the simulation for the tip displacement of the piezoelectric spiral.

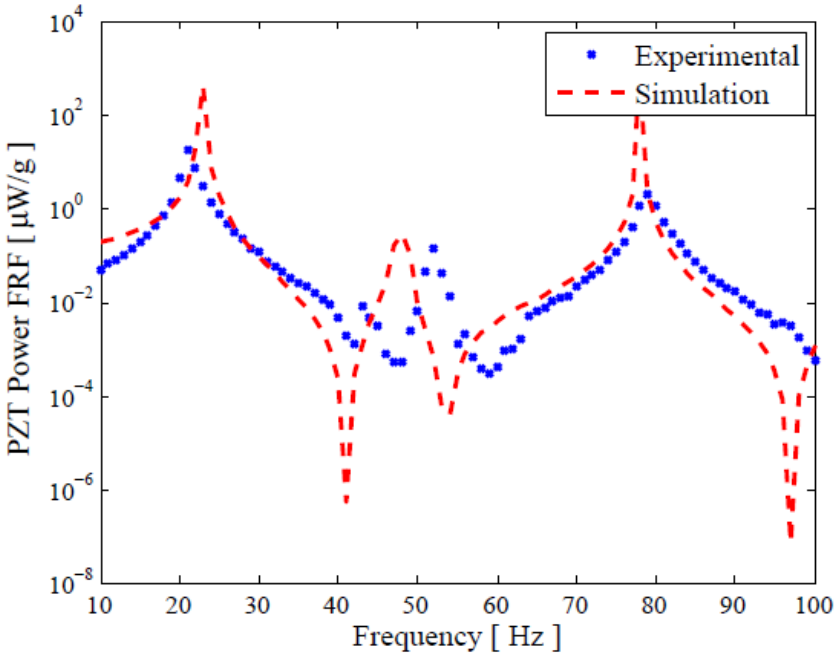

Figure 59: P-MAG results for the experimental vs. the simulation for the power output of the piezoelectric spiral.

The simulation of the power output from the magnet's motion was done separately from the piezoelectric. Figure 60 shows the results of the comparison. It is observed that the results are in agreement and the model closely represents the experiment.

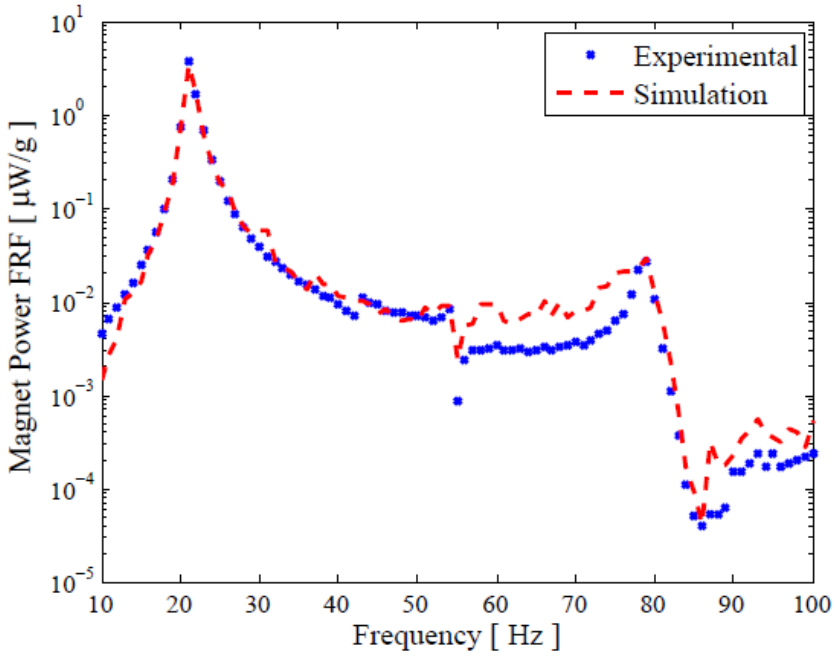

Figure 60: P-MAG results for the experimental vs. the simulation for the power output of the magnet.

The simulation and experimental results are in good agreement for the P-MSM and the P-MAG harvesters. This allows the simulation to accurately model experimental setups. This in turn allows for ease of designing and optimizing the harvesters for different applications.

6.4 Discussion

Currently in the field of energy harvesting there is not one single unified method for comparing the effectiveness of harvesters due to the large variations in the data that is presented in published works. This means some assumptions and calculations have to be made from the data provided. S. P. Beeby et al. [20] derived a measure for normalized power density (NPD) that was used only as an indication of relative performance. It is described as

$$NPD = \frac{P}{A^2 V} \tag{24}$$

where P is the peak power output, A is the base acceleration, and V is the volume of the harvester. Table 7 compares some available harvesters in the literature and their respective NPD information.

Table 7: Comparison with other published energy harvester.

Energy Harvesters	Frequency $[Hz]$	Acceleration $[m/s^2]$	Volume $[cm^3]$	Power $[\mu W]$	NPD $[kgs/m^3]$
P-MSM (presented research)	16-26	2.94	4.74	22	0.58
P-MAG (presented research)	21	2.94	1.66	52	15.38
Beeby [20]	52	0.589	0.15	46	883.97
Roundy [24]	120	2.5	1	375	60
Karami [38]	8	1.18	8.6	110	9.19
Wu [39]	N/A	12	0.0196	23.2	8.22
Ching [51]	110	95.5	1	830	0.09
White [52]	80	2.3	0.125	2.1	3.18
Jeon [53]	13900	106.8	0.000027	1	3.25

Table 7 shows a few harvesters that have higher NPD values than the P-MSM studied in this work. For example, Beeby et al. [20] has an NPD of 883 kgs/m^3 which is calculated using only the volume of the magnets. If the full volume of the harvester which includes the bulk volume of the magnets, the tungsten mass used to tune the frequency, and the cantilever beam was to be considered, this value would drop to around 70 kgs/m^3. Also the operating frequency is about 52 Hz which is in the higher frequency range and not practical for the application intended in this thesis. Roundy [24] and White [52] both have harvesters that operate at 120 Hz and 80 Hz respectively. Also, Jeon [53] and Wu [39] designed MEMS harvesters that operate in the kHz range. These frequencies are not practical for the applications intended in this thesis either. The P-MSM in comparison operates in frequencies under 26 Hz. Also, Karami [38] designed a harvester that operates at 8 Hz but it is large in size with the beam dimensions being 154 x 25 mm where the P-MSM has a 45 mm diameter, the volume is also almost double. Karami's [38] harvester has a bandwidth of about 2-3 Hz whereas the P-MSM has an operating range of 16-26 Hz.

Lower operating frequency, small dimensions as well as the bandwidth of the frequency operation (10 Hz) are among the advantages of the P-MSM harvesting unit fabricated in this research. The P-MAG harvester on the other hand, has a narrow frequency bandwidth about 21 Hz but has a higher power

output. Therefore, any small changes in the base excitation frequency from the peak value results in a significant drop in the power of the unit. This design may be pursued for cases where the ambient excitation frequency is fairly constant.

It should be noted that in general NPD is not an ideal measurement for harvesters of higher frequency bandwidth due to the power being measured only at the peak frequency. NPD depends highly on how the volume calculation was performed. Some works incorporate only the active volume, while others use the volume of the harvester as a whole. Nonetheless, it is only used as a guide for comparison.

Chapter 7: Conclusion and Future Work

7.1 Conclusion

Harvesting energy from ambient vibrations is a highly sought after method because of the wide range of available sources that produce vibration energy, from industrial machinery to human motion application. Substantial research has been performed on basic energy harvesting technologies such as electromagnetic, electrostatic, piezoelectric, and magnetostrictive technologies. Hybrid energy harvesters are a new class of harvesters that employ multiple commonly used harvester technologies into a single system. In this work, the design of two different hybrid energy harvesters was introduced.

The first prototype studied in this thesis was the P-MSM harvester, which is composed of both piezoelectric and magnetostrictive technologies. These two materials are both fabricated in a spiral shape and are allowed to resonate at different frequencies which results in a wide band range of operation. The second prototype was the P-MAG harvester, which is composed of piezoelectric and electromagnetic technologies. The piezoelectric layer used for this harvester also is made in to the spiral geometry. A magnet is attached to the center of the spiral, and a copper coil is employed for harvesting from the magnet.

Based on the results of this research, the conclusions can be presented as follows:

1. *The P-MSM harvester can operate at a wide band of frequencies*
   The piezoelectric and magnetostrictive layers resonate at different frequencies. This results in a harvester that is capable of operating between 16 Hz and 26 Hz, with a power output ranging from 2 $\mu W/g$ to 22 $\mu W/g$. This wide range of frequencies is very beneficial in applications where the ambient vibration is not consistent and shifts over time. It allows the harvester to still be operating at around the peak power output, even with the ambient frequency changing.

2. *The P-MAG harvester has the ability to produce a larger power output at a lower frequency compared to the P-MSM*
   The piezoelectric layer in the P-MSM harvester resonates at 23 Hz. The added weight of the magnet on the piezoelectric spiral in the P-MAG harvester results in the reduction of the resonance frequency to 21 Hz. Since the magnet is attached to the spiral it will also resonate at the same frequency. Therefore, the materials will both be harvesting the most energy at the same frequency which will allow for a much larger power output. This harvester has a peak

power output of 52 $\mu W/g$, which is more than double that produced by the P-MSM harvester. This harvester is ideal in situations where the ambient vibrations are consistently fixed at one frequency.

3. *The simulation and the experimental results are in good agreement*

   The two harvesters were subjected to a controlled sign sweep that was produced by a shaker and the resulting power output recorded. It was then compared with the results from simulations and showed good agreement. The simulation was able to model the torsional mode in the piezoelectric harvester with a 9% error, due to the complex geometry of the spiral beam. However, the bending modes were a more accurate representation of the experiment.

4. *Magnetostrictive material was shown to a be a viable energy harvesting technology*

   Magnetostrictive material is not commonly used in vibration energy harvesting application. Metglas is a magnetostrictive laminate that is produced in 25 μm thin sheets. 100 layers were cut, annealed and epoxied together in an effort to magnify the magneto-mechanical effect. It was successful in producing energy that is comparable to piezoelectric material as well as possessing high flexibility that allows for a low natural frequency (17 Hz).

5. *The spiral geometry greatly reduced the size of the harvester*

   The cantilever beam is the geometry that is commonly used in this field. The limitation arises when the beams dimensions get larger in order to have more active material for a higher power output or when the size is reduced (and thus, the natural frequency significantly increases). The spiral geometry allows for there to be a larger volume of active material while keeping the natural frequency relatively low. This is very beneficial for MEMS application where size is an important criterion of an effective energy harvester.

7.2 Future Work

In this work the two hybrid harvesters were modelled, fabricated, and tested. A continuation of the work in this thesis can be made as follows:

- Optimizing the P-MSM and the P-MAG power output. This can be achieved by tweaking the spiral geometry in an attempt to maximize the harvester's capability.

- Rectifying the signal coming out of the harvesters. In this work the electrical load was reduced to a resistor. Efforts should be made to rectify and store the output from the harvester, in order to allow for a sensor to be powered. The rectifier should be a passive rectifier that does not need any external power to operate, but should be as efficient as possible due to the small signal coming from the harvester.

- Lastly, scaling the design to MEMS scale. Energy harvesting for MEMS application is a field that received substantial attention from researchers. Efforts can be made towards decreasing the size of this harvester while still maintaining a reasonable natural frequency and power output. This can be achievable due to the properties of the spiral beam geometry.

References

[1] Mahmoud, M. A. E., Abdel-Rahman, E. M., El-Saadany, E. F, and Mansour, R. R. (2010). Electromechanical coupling in electrostatic micro-power generators. *Smart Materials and Structures*, 19 (2), 1-8.

[2] Mitcheson, P. D., Green, T. C., Yeatman, E. M., and Holmes A. S. (2004). Architectures for vibration-driven micropower generators. *Journal of Microelectromechanical Systems*, 13 (3), 429-440.

[3] Roundy S., Wright P. K. and Pister K. S. J. (2002). Micro-electrostatic vibration-to-electricity converters. *ASME International Mechanical Engineering Congress and Expostion*, New Orleans Louisuana.

[4] Khaligh, A., Zeng, P., and Zheng C. (2010). Kinetic energy harvesting using piezoelectric and electromagnetic technologies—state of the art. *IEEE Transactions on Industrial Electronics*, 57 (3), 850-860.

[5] Shearwood, C., and Yates, R. B. (1997). Development of an electromagnetic microgenerator. *IEE Electronics Letters*, 33 (22), 1883-1884.

[6] Arnold, D.P., Das, S., Cros, F., Zana, I., Allen, M.G., and Lang, J. H. (2006). Magnetic induction machines integrated into bulk-micromachined silicon. *Journal of Microelectromechanical Systems*, 15 (2), 406-414.

[7] Holmes, A.S., Hong G., and Pullen, K.R. (2005). Axial-flux permanent magnet machines for micropower generation. *Journal of Microelectromechanical Systems*, 14 (1), 406-414.

[8] Roundy, S., Wright, P. K., and Rabaey, J. (2003). A study of low level vibrations as a power source for wireless sensor nodes. *Computer Communications*, 26 (11) ,1131-1144.

[9] Mansour, M. O., Arafa, M. H., and Megahed, S. M. (2010). Resonator with magnetically adjustable natural frequency for vibration energy harvesting. *Sensors and Actuators A*, 163 (1), 297-303.

[10] Lefeuvre, E., Badel, A., Richard, C., and Guyomar, D. (2005). Piezoelectric energy harvesting device optimization by synchronous electric charge extraction. *Journal of Intelligent Material Systems and Structures*,16 (10), 865-876.

[11] Lu, F., Lee, H. P., and Lim S. P. (2004). Modeling and analysis of micro piezoelectric power generators for micro-electromechanical-systems applications. *Smart Materials and Structures*, 13 (1), 57-63.

[12] Wu, G., Zhang, R., Li, X., and Zhang, N. (2011). Resonance magnetoelectric effects in disk-ring (piezoelectric -magnetostrictive) composite structure. *Journal of Applied Physics*, 110 (12), 1-5.

[13] Li, L., Lin, Y. Q., and Chen, X. M. (2007). CoFe2O4/Pb(Zr052Ti0.48)O3 disk-ring magnetoelectric composite structures. *Journal of Applied Physics*, 102 (6), 1-4.

[14] Park, C., Cho, K., Arat, M. A., Evey, J., and Priya, S. (2010). High magnetic field sensitivity in Pb(Zr,Ti)O3–Pb(Mg1/3Nb2/3)O3 single crystal/Terfenol-D/Metglas magnetoelectric laminate composites. *Journal of Applied Physics*, 107 (9), 1-4.

[15] Zhao, X., and Lord, D. G. (2006). Application of the Villari effect to electric power harvesting. *Journal of Applied Physics*, 99 (8), 1-4.

[16] Saha, C. R., O'Donnell, T., Wang, N., and McCloskey, P. (2008). Electromagnetic generator for harvesting energy from human motion. *Sensors and Actuators A*, 147 (1), 248-253.

[17] Duffy, M. and Carroll, D.(2004). Electromagnetic generators for power harvesting. IEEE Power *Electronics Conference*, Aachen, Germany.

[18] El-Hami, M., Glynne-Jones, P., White, N. M., Hill, M., Beeby, S., James, E., Brown, A.D., and Ross, J.N. (2001). Design and fabrication of a new vibration-based electromechanical power generator. *Sensors and Actuators A*, 92 (1-3), 335-342.

[19] Glynne-Jones, P., Tudor, M. J., Beeby, S. P., and White, N. M. (2004). An electromagnetic, vibration-powered generator for intelligent sensor systems. *Sensors and Actuators A*, 110 (1-3), 344-349.

[20] Beeby, S. P., Torah, R. N., Tudor, M. J., Glynne-Jones, P., O'Donnell, T., Saha, C. R., and Roy, S. (2007). A micro electromagnetic generator for vibration energy harvesting. *Journal of Micromechanics and Microengineering,*17 (7), 1257-1265.

[21] Yang, B., Lee, C., Xiang, W., Xie, J., He, J. H., Kotlanka, R. K., Low, S. P., and Feng, H. (2009). Electromagnetic energy harvesting from vibrations of multiple frequencies. *Journal of Micromechanics and Microengineering,*19 (3), 1-8.

[22] Soliman, M., Abdel-Rahman, E. M., El-Saadany, E. F., and Mansour, R. R. (2009). A Design Procedure for Wideband Micropower Generators. *Journal of Microelectromechanical Systems*, 18 (6), 1288-1299.

[23] Sari, I., Balkan, T., Kulah, H. (2008). An electromagnetic micro power generator for wideband environmental vibrations. *Sensors and Actuators A*, 145–146, 405–413.

[24] Roundy, S., and Wright, P. K. (2004). A piezoelectric vibration based generator for wireless electronics. *Smart Materials and Structures*, 13 (5), 1131-1142.

[25] Jiang, S., Li, X., Guo, S., Hu, Y., Yang, J., and Jiang, Q. (2005). Performance of a piezoelectric bimorph for scavenging vibration energy. *Smart Materials and Structures*, 14 (4), 769-774.

[26] Yang, J., Zhou, H., Hu, Y., and Jiang Q. (2005). Performance of a Piezoelectric Harvester in Thickness-Stretch Mode of a Plate. *IEEE Transactions on Ultrasonics, Ferroelectrics, and Frequency Control*, 52 (10), 1872-1876.

[27] White, N. M., Glynne-Jones, P., and Beeby, S. P. (2001). A novel thick-film piezoelectric micro-generator. *Smart Materials and Structures*, 10 (4), 850-852.

[28] Challa, V. R., Prasad, M. G., Shi, Y., and Fisher, F. T. (2008). A vibration energy harvesting device with bidirectional resonance frequency tenability. *Smart Materials and Structures,*17 (1), 1-10.

[29] Leland E. S. and Wright P. K. (2006). Resonance tuning of piezoelectric vibration energy scavenging generators using compressive axial preload. *Smart Materials and Structures,*15 (5), 1413-1420.

[30] Hu, H., Xue, H., and Hu Y. (2007). A Spiral-Shaped Harvester with an Improved Harvesting Element and an Adaptive Storage Circuit. *IEEE Transactions on Ultrasonics, Ferroelectrics, and Frequency Control*, 54 (6), 1177-1187.

[31] Lan, J., Hu, L., Wang, H., Cheng, J., Hu, H. (2011). Numerical analysis on an annular bimorph piezoelectric power harvester with the out-of-plane vibration mode. *Piezoelectricity, Acoustic Waves and Device Applications*, Shenzhen, China.

[32] Paprotny, I., White, R. M., and Wright, P. K. Modeling, design and fabrication of a MEMS AC energy scavenger for smart grid applications. California Energy Commission.

[33] Ryu, J., Carazo, A.V., Uchino, K., and Kim, H. (2001). Magnetoelectric properties in piezoelectric and magnetostrictive laminate composites. *Japanese Journal of Applied Physics*, 402 (1), 4948-4951.

[34] Dong, S., Cheng, J., Li, J.F., and Viehland, D. (2003). Enhanced magnetoelectric effects in laminate composites of Terfenol-D/Pb(Zr,Ti)O3 under resonant drive. *Applied Physics Letters*, 83 (23), 4812.

[35] Dai,X., Wen, Y., Li, P., Yang, J., and Li, M. (2011).Energy harvesting from mechanical vibrations using multiple magnetostrictive/piezoelectric composite transducers. *Sensors and Actuators A,*166 (1), 94-101.

[36] Wang, L. and Yuan F. G. (2008). Vibration energy harvesting by magnetostrictive material. *Smart Materials and Structures*,17 (4), 1-14.

[37] Wischke, M., Masur, M., Goldschmidtboeing, F., and Woias, P. (2010). Electromagnetic vibration harvester with piezoelectrically tunable resonance frequency. *Journal of Micromechanics and Microengineering*, 20(3), 1-7.

[38] Karami, M.A. (2011). Micro-Scale and nonlinear vibrational energy harvesting. Virginia Polytechnic Institute and State University.

[39] Wu, X., Khaligh, A., and Xu, Y.(2008). Modeling, Design and optimization of hybrid electromagnetic and piezoelectric MEMS energy scavengers. *IEEE Custom Integrated Circuit Conference*, 177-180.

[40] Fang, H.B., Liu, J. Q., Xu, Z. Y., Dong, L., Wang, L., Chen, D., Cai, B. C., and Liu, Y. (2006). Fabrication and performance of MEMS-based piezoelectric power generator for vibration energy harvesting. *Microelectronics Journal*, 37 (11), 1280-1284.

[41] Roundy, S. (2005). On the effectiveness of vibration-based energy harvesting. *Journal of Intelligent Material Systems and Structures,*16 (10), 809-823.

[42] Gilbert, J. M. and Balouchi, F. (2008). Comparison of energy harvesting systems for wireless sensor networks. *International Journal of Automation and Computing*, 5 (4), 334-347.

[43] Cook-Cennault, K. A., Thambi, N., and Sastry, A. M. (2008). Powering MEMS portable devices—a review of non-regenerative and regenerative power supply systems with special emphasis on piezoelectric energy harvesting systems. *Smart Materials and Structures,*17 (4), 1-33.

[44] Donald J.L., (2007). Smart Material Systems. 1st ed. Hoboken, New Jersey: John Wiley and Sons Incorporated. p 162. Print.

[45] Piezo Systems Inc. PSI-5A4E piezoceramic sheets. [ONLINE] Available at: http://www.piezo.com/prodsheet1sq5A.html. [Last Accessed November 2013].

[46] Metglas Incorporated. 2605SA1 and 2605HB1 magnetic alloy. [ONLINE] Available at: http://www.metglas.com/products/magnetic_materials/2605SA1.asp. [Last Accessed November 2013].

[47] Metglas Incorporated. Amorphous alloys for transformer cores. [ONLINE] Available at: http://www.metglas.com/assets/pdf/2605sa1.pdf. [Last Accessed November 2013].

[48] K & J Magnetics Incorporated. Neodymium disk magnets D51-N52. [ONLINE] Available at: http://www.kjmagnetics.com/proddetail.asp?prod=D51-N52. [Last Accessed November 2013].

[49] Zhu, D., Tudor, M. J., and Beeby, S. P. (2010). Strategies for increasing the operating frequency range of vibration energy harvesters: a review. *Measurement Science and Technology*, 21 (2), 1-29.

[50] Inman, D. J. (2007). *Engineering vibration*. Upper Saddle River, New Jersey: Pearson Prentice Hall, p 547. Print.

[51] Ching, N.H., Wong, H. Y., Li, W. J., Leong, P. H. W., and Wen, Z. (2001). A laser-micromachined vibrational to electrical power transducer for wireless sensing systems. *Solid State Sensors and Actuators*, Munich, Germany, June 2001.

[52]Glynne-Jones, P., Beeby, S. P., and White, N.M. (2001). Towards a piezoelectric vibration-powered microgenerator. *IEE Science, Measurement and Technology*, 148 (2), 68-72.

[53] Jeona, I., Omiya, M., Kishimotob, K., Asahinaa, T., and Im, S. (2005). Modeling of a Gc-sensing element for the interfacial toughness of metal thin films on substrates. *Sensors and Actuators*,122 (2), 291-300.